Environmental Modelling & Software 35 (2012) 104–121

Contents lists available at SciVerse ScienceDirect

Environmental Modelling & Software

journal homepage: www.elsevier.com/locate/envsoft

Time-scale dependence in numerical simulations: Assessment of physical, chemical, and biological predictions in a stratified lake at temporal scales of hours to months

Emily L. Kara [a,*], Paul Hanson [b], David Hamilton [c], Matthew R. Hipsey [d], Katherine D. McMahon [a,e], Jordan S. Read [a], Luke Winslow [b], John Dedrick [b], Kevin Rose [f], Cayelan C. Carey [g], Stefan Bertilsson [h], David da Motta Marques [i], Lucas Beversdorf [a], Todd Miller [a], Chin Wu [a], Yi-Fang Hsieh [a], Evelyn Gaiser [j], Tim Kratz [b]

[a] Civil and Environmental Engineering Department, University of Wisconsin–Madison, 1415 Engineering Dr., Madison, WI 53706, USA
[b] Center for Limnology, University of Wisconsin–Madison, 680 N. Park St., Madison, WI 53706, USA
[c] Department of Biological Sciences, University of Waikato, Gate 1 Knighton Road, Hamilton 3240, New Zealand
[d] School of Earth and Environment, The University of Western Australia, 35 Stirling Highway, Crawley, WA 6009, Australia
[e] Department of Bacteriology, University of Wisconsin–Madison, 1550 Linden Dr., Madison, WI 53706, USA
[f] Smithsonian Environmental Research Center, 647 Contees Wharf Road, Edgewater, MD 21037, USA
[g] Department of Ecology and Evolutionary Biology, Cornell University, Ithaca, NY 14853, USA
[h] Department of Ecology, Genetics, and Limnology, Uppsala University, Norbyv. 18 D, 75236 Uppsala, Sweden
[i] Instituto de Pesquisa Hidráulicas, Universidade Federal do Rio Grande do Sul, Av. Bento Gonçalves 9500, Caixa Postal 15.029, 91501-970 Porto Alegre, RS, Brazil
[j] Department of Biological Sciences, Southeast Environmental Research Center, Miami, FL 33199, USA

ARTICLE INFO

Article history:
Received 21 March 2011
Received in revised form
14 February 2012
Accepted 15 February 2012
Available online 13 March 2012

Keywords:
Ecosystem modeling
Phytoplankton
Spectral analysis
Wavelet analysis
Automated observatory
Sensor network

ABSTRACT

We evaluated the predictive ability of a one-dimensional coupled hydrodynamic-biogeochemical model across multiple temporal scales using wavelet analysis and traditional goodness-of-fit metrics. High-frequency in situ automated sensor data and long-term manual observational data from Lake Mendota, Wisconsin, USA, were used to parameterize, calibrate, and evaluate model predictions. We focused specifically on short-term predictions of temperature, dissolved oxygen, and phytoplankton biomass over one season. Traditional goodness-of-fit metrics indicated more accurate prediction of physics than chemical or biological variables in the time domain. This was confirmed by wavelet analysis in both the time and frequency domains. For temperature, predicted and observed global wavelet spectra were closely related, while observed dissolved oxygen and chlorophyll fluorescence spectral characteristics were not reproduced by the model for key time scales, indicating that processes not modeled may be important drivers of the observed signal. Although the magnitude and timing of physical and biological changes were simulated adequately at the seasonal time scale through calibration, time scale-specific dynamics, for example short-term cycles, were difficult to reproduce, and were relatively insensitive to the effects of varying parameters. The use of wavelet analysis is novel to aquatic ecosystem modeling, is complementary to traditional goodness-of-fit metrics, and allows for assessment of variability at specific temporal scales. In this way, the effect of processes operating at distinct temporal scales can be isolated and better understood, both in situ and in silico. Wavelet transforms are particularly well suited for assessment of temporal and spatial heterogeneity when coupled to high-frequency data from automated in situ or remote sensing platforms.

© 2012 Elsevier Ltd. All rights reserved.

1. Introduction

Anthropogenic activity has resulted in a globally pervasive degradation of freshwater ecosystem services, such as the availability and quality of water for consumption, irrigation, and recreation. In lakes with high nutrient loads from surrounding landscapes, eutrophication is one of the leading concerns. Eutrophic lakes are characterized by frequent phytoplankton blooms that affect the esthetic nature of the lake, and may produce toxins that disrupt food webs and affect humans (Carmichael, 2002; Jonasson et al., 2010). Despite extensive research on phytoplankton

* Corresponding author.
E-mail address: kara@wisc.edu (E.L. Kara).

1364-8152/$ – see front matter © 2012 Elsevier Ltd. All rights reserved.
doi:10.1016/j.envsoft.2012.02.014

dynamics, the frequency and timing of phytoplankton blooms remain elusive to accurate prediction (Arhonditsis and Brett, 2004; Flynn, 2005a).

Numerical simulations are often used to predict the impact of environmental changes, including those imposed by climate, land-use, nutrient loading, and groundwater, on aquatic ecosystems (e.g. Arhonditsis and Brett, 2005a, b; Gal et al., 2009; Markensten et al., 2010; Trolle et al., 2011, 2008). Typically, models are calibrated to data from routine monitoring programs that sample the environment at fortnightly or monthly intervals, enabling simulations to reproduce seasonal and inter-annual variations. However, ecosystem phenomena relevant to water quality, such as phytoplankton succession and bloom formation, can occur over time scales of hours or days, and models calibrated exclusively to longer time scales may not provide adequate insight into the causes and consequences of these phenomena (Harris, 1987) as even for the same state variable, different drivers may dominate variability at different time scales (Hanson et al., 2006).

Advection, light, nutrients, and predation are among the drivers of spatial and temporal heterogeneity of phytoplankton populations. Aquatic ecosystem models such as DYRESM-CAEDYM (Gal et al., 2009), ELCOM-CAEDYM (Romero et al., 2004), PROTECH (Elliott et al., 2007), and PCLake (Janse et al., 2010) are designed to represent these processes and predict outcomes on phytoplankton populations, but validation at the lower end of ecologically relevant time and space scales (e.g. hours to days and meters to tens of meters), is frequently limited by the resolution of observed data. Recently, the assessment of modeling accuracy of spatial heterogeneity in phytoplankton has been facilitated by the use of in situ and remote sensing technologies (e.g. Alexander and Imberger, 2009; Fragoso et al., 2008), but similar assessments of variations at short time intervals (e.g., hours to days) are rare, in part due to the cost and effort associated with making high-frequency observations using traditional, manual means. However, high-frequency water quality variables including temperature, dissolved oxygen, and phytoplankton pigment fluorescence data are available for many lakes via sensor networks (Porter et al., 2009). Here, we use both manual and high-frequency data to assess a model intended to capture the critical physical–biogeochemical interactions driving phytoplankton dynamics. We assess model predictions in the time and frequency domains using wavelet analysis; the application of this technique is novel for the assessment of aquatic ecosystem models, and allows exploration of how model setup, structure, and parameterization affect predictions of variability across a range of temporal scales. We demonstrate that the advent of high-frequency automated sensor data from in situ lake observatories presents new opportunities and challenges for evaluating the predictive abilities of numerical simulations at temporal scales previously impossible.

2. Materials and methods

Lake Mendota, Wisconsin (WI) was chosen for this study because of its eutrophic status, extensive historical datasets, frequent manual water quality observations, and in situ sensor observatory. With some notable exceptions, summertime phytoplankton biomass in the lake is dominated by the Cyanobacteria genera *Microcystis* and *Aphanizomenon* (Brock, 1985; Carpenter et al., 2006). We chose to apply the model during this season (late June through late September 2008) because of availability of manual and high-frequency automated observations that could be used for comparative purposes with model simulation output.

The Dynamic Reservoir Simulation Model (DYRESM) was configured for Lake Mendota and coupled to the Computational Aquatic Ecosystem Dynamic Model (CAEDYM). DYRESM simulates the one-dimensional (1D) vertical structure of temperature, density, and salinity in a water body. CAEDYM is a process-based lake ecosystem model that simulates the time-varying distributions of carbon, nitrogen, phosphorus, dissolved oxygen, silica, phytoplankton and zooplankton. DYRESM and CAEDYM have been described elsewhere in detail (Gal et al., 2009; Imberger and Patterson, 1981).

2.1. Site description

Lake Mendota is located in Wisconsin, USA (43°06′24″N; 89°25′29″W) and has three main inflows, a single outflow, and a mean residence time of 4.5 years. The surface area is 39 km^2 and the mean and maximum depths are 12 and 25 m, respectively. The 686-km^2 watershed is dominated by agriculture, which has contributed significantly to the eutrophic status of the lake (Brock, 1985). The onset of eutrophication is considered to have occurred in the mid-1800s (Stewart, 1976) and has been the focus of scientific study for more than a century, starting with the work of Birge and Juday (Birge, 1915; Birge and Juday, 1911; Juday, 1914). Lake Mendota has comprehensive historical datasets and is a site of continuing long-term study (Beckel, 1987; Brock, 1985; Magnuson et al., 2006).

2.2. Observed data

Data for model calibration and validation were obtained from the North Temperate Lakes Long Term Ecological Research (NTL LTER) program, the University of Wisconsin Space Science and Engineering Ground-Based Atmospheric Monitoring Instrument Suite Rooftop Instrument Group (SSEC GAMIS RIG, located 1.2 km from south shore of Lake Mendota and ~3 km from location of instrumented buoy), the United States Geological Survey (USGS) and an automated, instrumented buoy located near the center of the lake. We utilized these sources and historical publications to derive model forcing data and parameters for the simulations presented here.

Meteorological data at the hourly frequency were used to drive simulations. Wind speed, short-wave radiation, percent cloud cover, air temperature, vapor pressure, and precipitation were acquired from the SSEC GAMIS RIG. Hypsometric data input included area and volume at 1-m elevation intervals (Kamarainen et al., 2009). Volumetric flow rates and water temperature of three major inflows were acquired from USGS stream gage data at daily frequency.

Biweekly manual observations from the NTL LTER were used to prescribe initial conditions and for calibration of the model (NTL-LTER, 2011a, b, c). Data from 1995–2008 were used to assist with setting parameters for sediment nutrient fluxes and water column nitrogen transformations. The dataset included biweekly or monthly measurements of $NO_3^- - N$ (NO_3^- hereafter), $NH_4^+ - N$ (NH_4^+ here after), $PO_4^{3-}P$ (PO_4^{3-} hereafter), dissolved organic carbon (DOC), dissolved inorganic carbon (DIC), total nitrogen (TN), and total phosphorus (TP), at 0, 4, 8, 12, 16, and 20 m depths; temperature, pH, and dissolved oxygen (DO) every meter from 0 to 20 m; In 2008, weekly measurements of NO_3^-, PO_4^{3-}, TN, TP, DOC, DIC, and solvent-extracted chlorophyll-*a* (chl-*a*) at depths 0.5, 5, 10, 14, and 20 m were made. Depth integrated (0–8 m) samples were preserved biweekly and enumerated for phytoplankton cell counts by species and biovolume, and zooplankton counts by species and length. To align measurements of biomass of phytoplankton and zooplankton species with the partitioning in model simulations, phytoplankton and zooplankton counts were binned into one of four functional groups corresponding to groups of ecological coherence. For each sample, a minimum of 400 natural units per sample were counted and each sample was counted until the standard error of the mean of total cell counts was less than 10%. Phytoplankton biovolume and zooplankton mean lengths were converted to units of carbon concentration (g C m^{-3}) using conversion factors from the literature specific to functional groups (Table 1).

Automated high-frequency (min^{-1}) observations of temperature, DO, and chlorophyll fluorescence were made from an instrumented buoy platform at the deepest point in Lake Mendota (Figs. 1a–c and 2a). A thermistor chain measured water temperature at 0.5 m increments from 0 to 2 m and 1 m increments from 2 to 20 m depths (Apprise Templine, Duluth, MN), which was used to prescribe initial conditions for model simulations and was used to evaluate model performance for water temperature simulations. Dissolved oxygen (D-Opto, Zebra-tech Ltd., Nelson, New Zealand) and fluorescence (Cyclops-7 Chlorophyll Fluorometer, Turner Designs, Sunnyvale, CA) sensors were positioned at 0.5 m depth. After aggregation from min^{-1} to $hour^{-1}$ frequency to match model output, high-frequency temperature, DO, and chl-*a* fluorescence data were used for comparison against high-frequency model output of temperature, dissolved oxygen, and biomass expressed as chlorophyll-*a*. For chlorophyll fluorescence, the raw voltage output with the fluorometer default auto-gain was used; hereafter we refer to this measure as chl-*a* fluorescence in relative fluorescence units (RFU).

For each inflow, water samples were collected over the hydrograph to generate a total phosphorus (TP)-discharge relationship. Daily TP mass loading for 2008 was calculated using the USGS Graphical Constituent Loading Analysis System (GCLAS, Koltun et al., 2006). Average base-flow TP and dissolved inorganic phosphorus (PO_4^{3-}) concentrations specific to each inflow have been measured previously (Lathrop, 1979). We assumed the difference between TP and PO_4^{3-} concentrations was dominated by particulates (Lean, 1973a, b; Wetzel, 2001), and further specified to be organic in composition. A sensitivity analysis of chemical and biological response to the specific forms of P in hydrologic inflows was performed (e.g. the difference between TP and PO_4^{3-} defined as dissolved P, particulate P, particulate inorganic P, etc), and was found to have little effect on phytoplankton biomass and the chemical variables highlighted in this study, likely due to the small contribution of external TP loading to the in-lake P mass. We also tested the sensitivity of key state variables to both a range of historical P loading and a range of early summer

Table 1
General (A), bacterial (B), phytoplankton (C) and zooplankton (D) parameters used for the CAEDYM simulations, with modifications after Gal et al. (2009).

Parameter	Description	Units	Assigned value	Values from field/literature
(A) *General parameters*				
K_d	Light extinction coefficient of pure water	m^{-1}	0.25	
K_{PAR}	Fraction of incoming solar radiation which is photosynthetically active	–	0.45	
K_{eDOC}	Specific light attenuation coefficient due to the action of labile DOC	m^{-1} (gC m^{-3})$^{-1}$	0.02	0.02[i]
K_{eDOC}	Specific light attenuation coefficient due to the action of refractory DOC	m^{-1} (gC m^{-3})$^{-1}$	0.001	0.001[ii]
K_{ePOC}	Specific light attenuation coefficient due to the action of labile POC	m^{-1} (gC m^{-3})$^{-1}$	0.01	0.01[i]
K_{ePOC}	Specific light attenuation coefficient due to the action of refractory POC	m^{-1} (gC m^{-3})$^{-1}$	0.02	
k_{SOD}	Maximum sediment oxygen demand (SOD) at 20 °C	g m^{-2} day^{-1}	0.46	0.918[iii], 7.97[iv]
$k_{DO_{SOD}}$	Half saturation constant for DO effect on SOD	g DO m^{-3}	1.5	1.5[iv], 0.5[iii]
ϑ_{SOD}	Temperature multiplier for SOD	–	1.08	1.02–1.14[v]
DO^{atm}	Equivalent DO at the air–water interface	g DO m^{-3}	Equation	$Do^{atm} = f(p,T,S)$[v]
k_{O_2}	Oxygen transfer coefficient dependent on wind speed	m s^{-1}	Equation	$k_{O_2} = f(u,T,S)$[v]
PCO_2^{atm}	Partial pressure of CO_2 at the air–water interface	atm	350×10^{-6}	
k_{pCO_2}	Gas transfer velocity for CO_2	m s^{-1}	Equation	$k_{pCO_2} = f(u,T,S)$[v]
K_w	Ion product of water		Equation	$K_w = f(T)$[vi]
K_{a1};K_{a2}	First and second acidity constants		Equation	$K_{a1,2} = f(T)$[vi]
Y_{O_2C}	Stoichiometric ratio of DO to C during photosynthesis and respiration	g DO (g C)$^{-1}$	2.67	Stoichiometric relationship
Y_{O_2N}	Stoichiometric ratio of DO to N during nitrification	g DO (g N)$^{-1}$	3.43	Stoichiometric relationship
$V_{s_{POM}}$	Settling velocity of particulate detritus (POM), used for POC, PON, POP	m s^{-1}	Equation	Calculated from Stoke's Law: $V_{s_{POM}} = \frac{g d_{POM}^2}{18\nu}(\rho_{POM} - \rho_w)$
d_{POM}	Diameter of POM particles	m	8×10^{-5}	
ρ_{POM}	Density of POM particles	kg m^{-3}	1040	1070[vii]
$\mu_{DEC_{POC}}$	Maximum rate of POC decomposition to DOC at 20 °C	day^{-1}	0.070	0.0187 (benthic)[viii]
$\mu_{DEC_{POP}}$	Maximum rate of POP decomposition to DOP at 20 °C	day^{-1}	0.030	0.01–0.1[ix]
$\mu_{DEC_{PON}}$	Maximum rate of PON decomposition to DON at 20 °C	day^{-1}	0.035	0.01–0.03i[x]
k_{den}	Maximum denitrification rate under anoxia at 20 °C	day^{-1}	0.05	0.1i[x]
ϑ_{den}	Temperature multiplier for denitrification	–	1.05	1.045[viii]
K_{den}	Half saturation constant for denitrification dependence on oxygen	g DO m^{-3}	0.4	0.4i[x]
k_{nit}	Maximum nitrification rate under oxygen saturation at 20 °C	day^{-1}	0.106	0.106[iv], 0.1–0.2i[x]
ϑ_{nit}	Temperature multiplier for nitrification	–	1.08	1.08i[x]
K_{nit}	Half saturation constant for nitrification dependence on oxygen	g DO m^{-3}	1.5	1.5[iv]
ϑ_S	Temperature multiplier for sediment nutrient fluxes	–	1.08	
S_{FRP}	Maximum release rate of PO_4 from sediments at 20 °C	g m^{-2} day^{-1}	0.0125	0.03[iv], 0.065[x], 0.0008[xi]
$K_{DO_{FRP}}$	Half saturation constant for sediment PO_4 release dependence on DO	g DO m^{-3}	2.0	2.0[iv]
S_{NH_4}	Maximum release rate of NH_4 from sediments at 20 °C	g m^{-2} day^{-1}	0.31	0.31[iv]
$K_{DO_{NH\ 4}}$	Half saturation constant for sediment NH_4 release dependence on DO	g DO m^{-3}	2.0	2.0[iv], 0.025[xi]
S_{NO_3}	Maximum release rate of NO_3 from sediments at 20 °C	g m^{-2} day^{-1}	−0.12	−0.12[iv]
$K_{DO_{NO\ 3}}$	Half saturation constant for sediment NH_4 release dependence on DO	g DO m^{-3}	50	50[iv]
S_{DOC}	Maximum release rate of DOC from sediments at 20 °C	g m^{-2} day^{-1}	0.0	0.0[iv]
S_{DOC}	Maximum release rate of DOP from sediments at 20 °C	g m^{-2} day^{-1}	0.0	0.0[iv]
S_{DOC}	Maximum release rate of DON from sediments at 20 °C	g m^{-2} day^{-1}	0.0	0.0[iv]
$K_{DO_{DOC}}$	Half sat constant for sediment DOC release dependence on DO	g DO m^{-3}	0.5	0.5[iv]
(B) *Bacterial parameters*				
ϑ_B	Temperature multiplier for growth	–	1.08	
T_{STD_B}	Standard temperature	°C	20	
T_{OPT_B}	Optimum temperature	°C	30	30[xii]
T_{MAX_B}	Maximum temperature	°C	38	38[xii]
K_{DO_B}	Half saturation constant for dependence of POM/DOM decomposition on DO	g DO m^{-3}	1.5	
f_{An_B}	Aerobic/anaerobic factor	–	0.8	
ϑ_{Br}	Temperature multiplier for loss	–	1.08	
k_{Br}	Bacterial respiration rate at 20 °C	day^{-1}	0.12	
k_{Be}	DOC Excretion	–	0.7	
K_B	Half saturation constant for bacteria function	g C m^{-3}	0.01	
$\mu_{DEC_{DOC}}$	Maximum bacterial DOC uptake rate	day^{-1}	0.05	
k_{BIN}	Internal C:N ratio of bacteria	g N (g C)$^{-1}$	0.16	0.16[xiii]
k_{BIP}	Internal C:P ratio of bacteria	g P (g C)$^{-1}$	0.04	0.04[xiii]

Parameter	Description	Units	Assigned values				Values from field/literature			
			A_{Mic}: *Microcystis*	A_{Aph}: *Aphanizomenon*/ *Anabaena*	A_{Chlor}: *Chlorophytes*/ *Chrysophytes*	A_{Diat}: *Diatoms*	A_{Mic}: *Microcystis*	A_{Aph}: *Aphanizomenon*/ *Anabaena*	A_{Chlor}: *Chlorophytes*/ *Chrysophytes*	A_{Diat}: *Diatoms*
(C) *Phytoplankton parameters*										
μ_{MAx}	Maximum potential growth rate	day^{-1}	0.6	0.48	0.2	1.25	0.048–1.11[xiv]	0.27–0.98[xv] 0.27–1.56[xvi]	2.4–8.57[xvii] 0.62–2.91[xiv] 0.33–0.55[xviii]	1.7[xix]
I_s	Light saturation for maximum production	$\mu mol\ m^{-2}\ s^{-1}$	250	220	170	20			75[i]	
K_{eA}	Specific attenuation coefficient	$m^{-1}\ (gC\ m^{-3})^{-1}$	0.198	0.198	0.198	0.198				0.448[xx]
K_P	Half saturation constant for phosphorus uptake	$g\ P\ m^{-3}$	0.0018	0.0012	0.01	0.005			0.0011[xxi] 0.001[xxii]	0.0028–0.0111[xxi]
K_N	Half saturation constant for nitrogen uptake	$g\ N\ m^{-3}$	0.02	0.001	0.030	0.060				
IN_{MIN}	Minimum internal N ratio	$g\ N\ (g\ C)^{-1}$	0.070	0.070	0.090	0.090	0.163[xiv]	0.163[xiv]	0.034[xiv]	0.125[xxi]
IN_{MAx}	Maximum internal N ratio	$g\ N\ (g\ C)^{-1}$	0.24	0.16	0.14	0.15	0.239[xiv]	0.239[xiv]	0.135[xiv]	0.146[xxi]
UN_{MAx}	Maximum rate of nitrogen uptake	$g\ N\ (g\ C)^{-1}\ day^{-1}$	0.08	0.12	0.060	0.15				
IP_{MIN}	Minimum internal P ratio	$g\ P\ (g\ C)^{-1}$	0.002	0.005	0.006	0.021	0.014[xiv]	0.014[xiv]	0.021[xiv]	0.0119[xxi]
IP_{MAx}	Maximum internal P ratio	$g\ P\ (g\ C)^{-1}$	0.023	0.023	0.059	0.085	0.023[xiv]	0.023[xiv]	0.059[xiv]	0.085[xxi]
UP_{MAx}	Maximum rate of phosphorus uptake	$g\ P\ (g\ C)^{-1}\ day^{-1}$	0.01	0.01	0.007	0.018	0.01[xxiii]		0.0074[xxi]	0.0031–0.0187[xxi]
k_{NF}	N fixation rate	$g\ N\ (g\ C)^{-1}\ day^{-1}$	0	0.15	0	0	0	0.140[xxiv]	0	0
f_{NF}	Growth reduction under N_2 fixation	–	1.00	0.67	1.00	1.00				
ϑ_{Ag}	Temperature multiplier for growth	–	1.07	1.10	1.08	1.08	1.075[xxv]		1.075[xxv]	
T_{STD_A}	Standard temperature	°C	19	24	20	19				
T_{OPT_A}	Optimum temperature	°C	30	30	21	17	20–30[xxi] 29–34[xxvi]	25[xiv]	14–28[xxvii] 14–25[xli], 20[xxviii]	16–17[xxi]
T_{MAX_A}	Maximum temperature	°C	40	40	35	22	35[xxvi]	30[xiv]	29–35[xxvii], >35[xxi]	26–27[xxi]
k_r	Metabolic loss rate coefficient	day^{-1}	0.05	0.05	0.05	0.05	0.08[xxix]		0.07[xliii]	0.039–0.051[xxi] 0.01[xliii]
ϑ_{Ar}	Temperature multiplier for metabolic loss	–	1.10	1.09	1.06	1.08			1.05[xxv]	
k_{pr}	Rate of photorespiration (day^{-1})	–	0.014	0.014	0.014	0.014				
f_{res}	Fraction of respiration relative to total metabolic loss	–	0.8	0.8	0.8	0.5				
f_{DOM}	Fraction of metabolic loss rate that goes to DOM	–	0.3	0.1	0.1	0.5				
d_A	Cell diameter	m	1×10^{-5}	1×10^{-7}	1×10^{-5}	1×10^{-5}				
V_{S_A}	Settling velocity	$m\ s^{-1}$	3.6×10^{-5}	-5.1×10^{-7}	1.2×10^{-6}	−0.057				7×10^{-6} -1.2×10^{-5}[xxi]
Y_{ChlC}	Chlorophyll:C ratio	–	50	100	40	40				
$Y_{CBiovol}$	Carbon:biovolume ratio (used for estimating algal biomass gC/m^3)	$pg\ C\ \mu m^{-3}$	0.127	0.127	0.198	0.199	0.127[xiv]	0.127[xiv]	0.198[xiv]	0.199[xiv]

Parameter	Description	Units	Assigned values				Values from field/literature			
			Z_1: *Predatory*	Z_2: *Macro-large*	Z_3: *Macro-small*	Z_4: *Micro*	Z_1: *Predatory*	Z_2: *Macro-large*	Z_3: *Macro-small*	Z_4: *Micro*
(D) *Zooplankton parameters*										
g_{MAx}	Grazing rate	$gC\ m^{-3}\ (g\ Z\ m^{-3})^{-1}\ day^{-1}$	1	0.75	0.3	0.5	1[xxx]	0.75[xxxi] 1.67[xxxii]	0.3[xxxi]	
k_{mf}	Grazing efficiency	–	0.8	0.7	0.8	0.85				
k_{Zr}	Respiration rate coefficient	day^{-1}	0.1	0.2	0.075	0.025	0.32[xxx]	0.12[xxxii] 0.195[xxxiii]	0.06[xxxiv]	
k_{Zm}	Mortality rate coefficient	day^{-1}	0.02	0.04	0.015	0.005				
k_{Zf}	Fecal pellet fraction of grazing	day^{-1}	0.025	0.05	0.02	0.007				
k_{Ze}	Excretion fraction of grazing	day^{-1}	0.1	0.1	0.1	0.1	0.13[xxx]	0.11[xxxii]		
$f_{f_{SED}}$	Fecal pellet fraction that sinks directly to sediments	–	0.7	0.1	0.1	0.1				
ϑ_{Zg}	Temperature multiplier for growth	–	1.07	1.07	1.07	1.07	1.1[xxx]	1.15[xxxii]		
T_{STD_Z}	Standard temperature	°C	20	20	20	20	20[xxx]	20[xxxii]	20[xxx]	20[xxxv]
T_{OPT_Z}	Optimum temperature	°C	19	20	18	24	29[xxx] 11[xxxvi]	28[xxxii] 17[xxxvi]	17[xxxvi]	25[xxxv]
T_{MAX_Z}	Maximum temperature	°C	35	35	35	35	34[xxx]	34[xxxii]		

(*continued on next page*)

Table 1 (*continued*)

Parameter	Description	Units	Assigned values				Values from field/literature			
			Z_1: *Predatory*	Z_2: *Macro-large*	Z_3: *Macro-small*	Z_4: *Micro*	Z_1: *Predatory*	Z_2: *Macro-large*	Z_3: *Macro-small*	Z_4: *Micro*
ϑ_{Zr}	Respiration temperature dependence	–	1.11	1.15	1.06	1.06	1.1^{xxx}	1.15^{xxxii}		
K_Z	Half saturation constant for grazing	g C m^{-3}	2	2	2	2	0.14^{xxxvii}	$0.54^{xxxviii}$		0.164^{xxxix}
k_{ZIN}	Internal ratio of nitrogen to carbon.	g N (g C)$^{-1}$	0.18	0.18	0.16	0.15	0.184^{xl}	0.18^{xli}	0.161^{xlii}	0.149^{xliii}
							0.18^{xli}		0.114^{xli}	
k_{ZIP}	Internal ratio of phosphorus to carbon	g P (g C)$^{-1}$	0.0045	0.0125	0.006	0.03	0.005^{xl}	0.012^{xl}	0.0083^{xlii}	0.0212^{xliii}
							0.004^{xli}	0.0125^{xli}	0.0066^{xli}	
P_{Zk_1}	Preference of zooplankton for predatory zooplankton	–	0.15	0	0	0	0.1^{xliv}	$0^{xliv, xlv}$	0^{xlv}	0^{xlv}
P_{Zk_2}	Preference of zooplankton for macro-large zooplankton	–	0.15	0	0	0	$0.6^{xliv,xlv}$	$0^{xliv,xlv}$	0^{xlv}	0^{xlv}
P_{Zk_3}	Preference of zooplankton for macro-small zooplankton	–	0.15	0	0	0	$0.15^{xliv,xlv}$	0^{xlv}	0^{p}	0^{xlv}
P_{Zu_4}	Preference of zooplankton for micro-zooplankton	–	0.15	0	0	0	$0.15^{xliv,xlv}$	$0^{xliv,xlv}$	0^{xlv}	0^{xlv}
P_{Zp}	Preference of zooplankton for POC	–	0	0.1	0.098	0.05	0^{xlv}	0.1^{xlvi}	0.098^{xlvii}	
P_{Zb}	Preference of zooplankton for Bacteria	–	0	0.6	0.06	0.06	0^{xlv}	0.15^{xlvii}	0.6^{xlvii}	0.05^{xlvii}
$P_{A\ Mic}$	Preference of zooplankton for *Microcystis*-like phyto	–	0	0.01	0.001	0.05	0^{xlv}	0.01^{xlviii}	0.001^{xlvii}	0.05^{xlviii}
$P_{A\ Aph}$	Preference of zooplankton for *Aphaniazomenon*-like phyto	–	0	0.01	0.001	0.05	0^{xlv}	0.01^{xlix}	0.001^{xlvii}	0.05^{xlvii}
$P_{A\ Chlor}$	Preference of zooplankton for Chloro/chryso-like phyto	–	0	0.15	0.075	0.05	0^{xlv}	0.15^{xlix}	0.075^{xlvii}	0.05^{xlix}
$P_{A\ Diat}$	Preference of zooplankton for diatom-like phyto	–	0	0.18	0.075	0.05	0^{xlv}	0.18^{xlix}	0.075^{xlvii}	0.05^{l}
Min_{res}	Minimum phytoplankton biomass below which zooplankton will not graze	g C m^{-3}	0.01	0.03	0.8	0.05				

Sources: [i]Kirk, 1994; [ii]Morris et al., 1995; [iii]Brock, 1985; [iv]Derived from NTL LTER data specific to Lake Mendota; [v]Wanninkhof, 1992; [vi]Butler, 1982; [vii]Degobbis and Gilmartin, 1990; [viii]Sinsabaugh and Findlay, 1995; [ix]Jorgensen and Bendoricchio, 2001; [x]Holdren and Armstrong, 1980; [xi]Serruya et al., 1974; [xii]Lovell and Konopka, 1985; [xiii]Makino and Cotner, 2004; [xiv]Reynolds 2006; [xv]Foy et al., 1976; [xvi]Fogg, 1949; [xvii]Pollingher and Berman, 1982; [xviii]Sandgren, 1988; [xix]Butterwick et al., 2005; [xx]Kirk, 1994; [xxi]Zohary, unpublished data (after Gal et al., 2009); [xxii]Sandgren, 1988; [xxiii]Healey and Hendzel, 1979; [xxiv]Dugdale and Dugdale, 1962; [xxv]Hipsey, unpublished; [xxvi]Imai et al., 2009; [xxvii]Ukeles, 1961; [xxviii]Sandgren, 1995; [xxix]Robson and Hamilton, 2004; [xxx]Gophen, 1976a; [xxxi]Demott, 1982; [xxxii]Gophen, 1976b; [xxxiii]Lampert, 1986; [xxxiv]Urabe and Watanabe, 1990; [xxxv]Galkovskaja, 1987; [xxxvi]Bertilsson et al., 1995; [xxxvii]Landry and Hassett, 1985; [xxxviii]Haney and Trout, 1985; [xxxix]Stemberger and Gilbert, 1985; [xl]Andersen and Hessen, 1991; [xli]Sterner and Hessen, 1994; [xlii]Dobberfuhl and Elser, 2000; [xliii]Jensen and Verschoor, 2004; [xliv]Gophen and Azoulay, 2002; [xlv]Lampert, 2007; [xlvi]Lampert, 1974; [xlvii]Hadas et al., 1998; [xlviii]Scavia et al., 1988; [xlix]Hamels et al., 2004; [l]Madoni et al., 1990.

PO_4^{3-} concentrations, and found phytoplankton biomass was very sensitive to in-lake PO_4^{3-} initial conditions, while effects of P external loading was negligible (results not shown). The inflow-specific proportions of PO_4^{3-} to particulate organic P were applied to TP loading estimated by GCLAS.

Nitrogen load data for the year 2008 was not available, thus TN load was estimated by assuming an approximately constant mass ratio of TN:TP in inflows as has been observed historically in inflows to this lake (Lathrop, 1979). A range of annual TN load (520,000–1,150,000 kg N yr^{-1}) to Lake Mendota was estimated by Sonzogni and Lee as reported by Brock (1985). We assumed the ratio of 2008 TN load to the historical maximum TN load (1,150,000 kg N yr^{-1}) in any single year was proportional to the ratio of 2008 TP load (50,700 kg P yr^{-1}) to the maximum recorded annual TP load since 1976 (1994: 67,000 kg P yr^{-1}; (Lathrop et al., 1999)). Thus, TN load for 2008 was estimated to be 522,000 kg N yr^{-1}. The ratio of total nitrogen, inorganic N (NO_3^- and NH_4^+), and organic N for each inflow have been measured previously (Lathrop, 1979) and we assumed that the same ratio amongst species existed in 2008. Similar to external P loading and in-lake initial conditions, we also tested sensitivity of key state variables to external TN loading and in-lake TN initial conditions and found initial conditions to be much more important for subsequent predictions of phytoplankton biomass and chlorophyll than external TN loading (results not shown).

2.3. Model configuration

We initialized DYRESM-CAEDYM on day 179 of 2008 (June 27 2008) and simulated a 90 d period. Initial conditions for day 0 were based on observed data and exogenous drivers (e.g. prescribed daily meteorology, inflows and outflows) controlled subsequent dynamics. State variables were not reset to observed data at any time during the simulation. Minimum and maximum model vertical layer resolution was 0.5 and 2 m respectively, and the calculation and output time steps were 1 h.

The CAEDYM model was configured with four functional groups of phytoplankton, four zooplankton groups, and one bacterial functional group. For phytoplankton and zooplankton, functional groups were chosen to represent broader taxonomical groups of the most abundant phytoplankton and zooplankton in Lake Mendota for the modeled season and these also largely correspond to groups of ecological coherence. For phytoplankton functional groups, we included a nitrogen-fixing cyanobacteria genus represented by *Aphanizomenon* sp. (A_{Aph}), a non nitrogen-fixing cyanobacteria genus represented by *Microcystis* sp. (A_{Mic}), chlorophytes and chrysophytes (A_{Chlor}), and diatoms (A_{Diat}). Four zooplankton groups were modeled: predatory zooplankton (e.g. copepods, Z_{Cop}), large zooplankton (e.g. daphnia, Z_{Daph}), small zooplankton (e.g. small cladocerans, Z_{Clad}), and micro-zooplankton (e.g. rotifers, Z_{Rot}). Phytoplankton were configured with fixed internal carbon concentration (*IC*) and fixed carbon to chlorophyll-*a* ratio. One bacterial functional group was activated in the biogeochemical model, configured to assimilate organic C, N, and P and release excess C, N, and P in inorganic forms.

2.4. Parameterization

Literature values, estimates from observed data, and user-defined values comprised the chemical and biological parameter set, specific to Lake Mendota, which was adapted for this system based on a parameter set used by Gal et al. (2009). Site-specific parameters were used when possible. When no site-specific parameters were available, we used values based on those from the literature. We summarize abbreviations, descriptions, values and sources for general parameters (Table 1a), bacteria (Table 1b), phytoplankton (Table 1c) and zooplankton (Table 1d). Zooplankton observed mean lengths from NTL LTER database were converted to dry weight using empirical relationships specific to the four defined functional groups (Culver et al., 1985; McCauley, 1984; Ventura et al., 2000; Wiebe et al., 1975). Phytoplankton were parameterized with functional group-specific biomass to carbon ratios (Table 1c) while zooplankton was assumed to be 33% C by dry weight (Wiebe et al., 1975).

2.4.1. Light attenuation

Modeled chemical and biological feedback to hydrodynamic driver variables includes light attenuation from pure water, phytoplankton, dissolved and particulate organic material, and suspended inorganic materials; these variables contribute to vertical attenuation as a function of their simulated concentrations at each model time step. We estimated coefficients for DOC extinction (K_{eDOC}) and phytoplankton groups (K_{eP}) from observed data, and assumed a negligible effect by other non-phytoplankton particulate material and dissolved inorganic materials. We assume a linear relationship between chromophoric dissolved organic matter (CDOM) and DOC.

Photosynthetically active radiation (PAR, 400–700 nm) diffuse attenuation coefficients ($K_{d\ PAR}$) were calculated from observed Secchi disk depth (z_s) for the 2008 ice-free season. For each z_s, $K_{d\ PAR}$ was estimated (Kirk, 1994):

$$K_{d\ PAR} = 1.7/z_s \quad (1)$$

We examined the linear relationship between phytoplankton functional group biomass (g C m^{-3}) and the estimated $K_{d\ PAR}$ (m^{-1}) for each observation, and

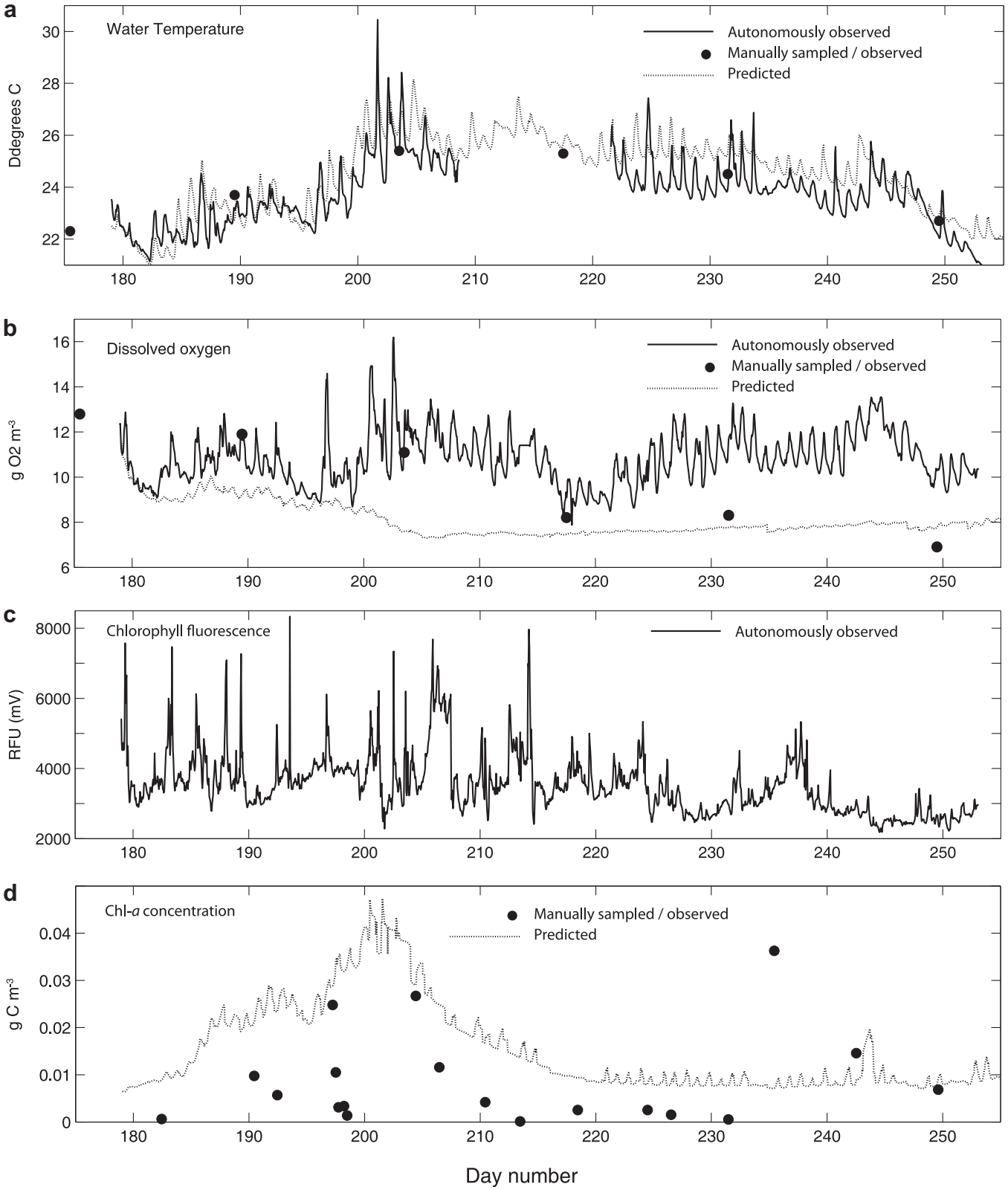

Fig. 1. High-frequency observed (solid) and predicted (dashed) temperature (a), dissolved oxygen (b) and chl-*a* fluorescence (c) and concentration (d). Predicted values were from the 0.5 m depth layer of the simulation. High-frequency observations (a, b, and c) were collected at an instrumented buoy (0.5 m depth) located near the center of Lake Mendota, WI from day number 180 to 270, 2008. Manual temperature, DO, and in vitro solvent −extracted chl-*a* measurements are overlaid as solid circles.

differentiated the attenuation imparted by constituent materials. We tested for significance between phytoplankton functional group biomass (g C m^{-3}) and estimated $K_{d\ PAR}$ (m^{-1}) in order to assign a specific K_d for each phytoplankton functional group, using 13 observations from 2008. Only the N-fixing functional group biomass showed a significant linear relationship ($r^2 = 0.37$, $p < 0.05$) with $K_{d\ PAR}$, but there was also a significant relationship between total phytoplankton biomass and $K_{d\ PAR}$ for the 2008 season ($R^2 = 0.59$, $p < 0.01$). Therefore, we assumed the uniform $K_{d\ PAR}$ per unit total phytoplankton biomass applied to all four phytoplankton functional

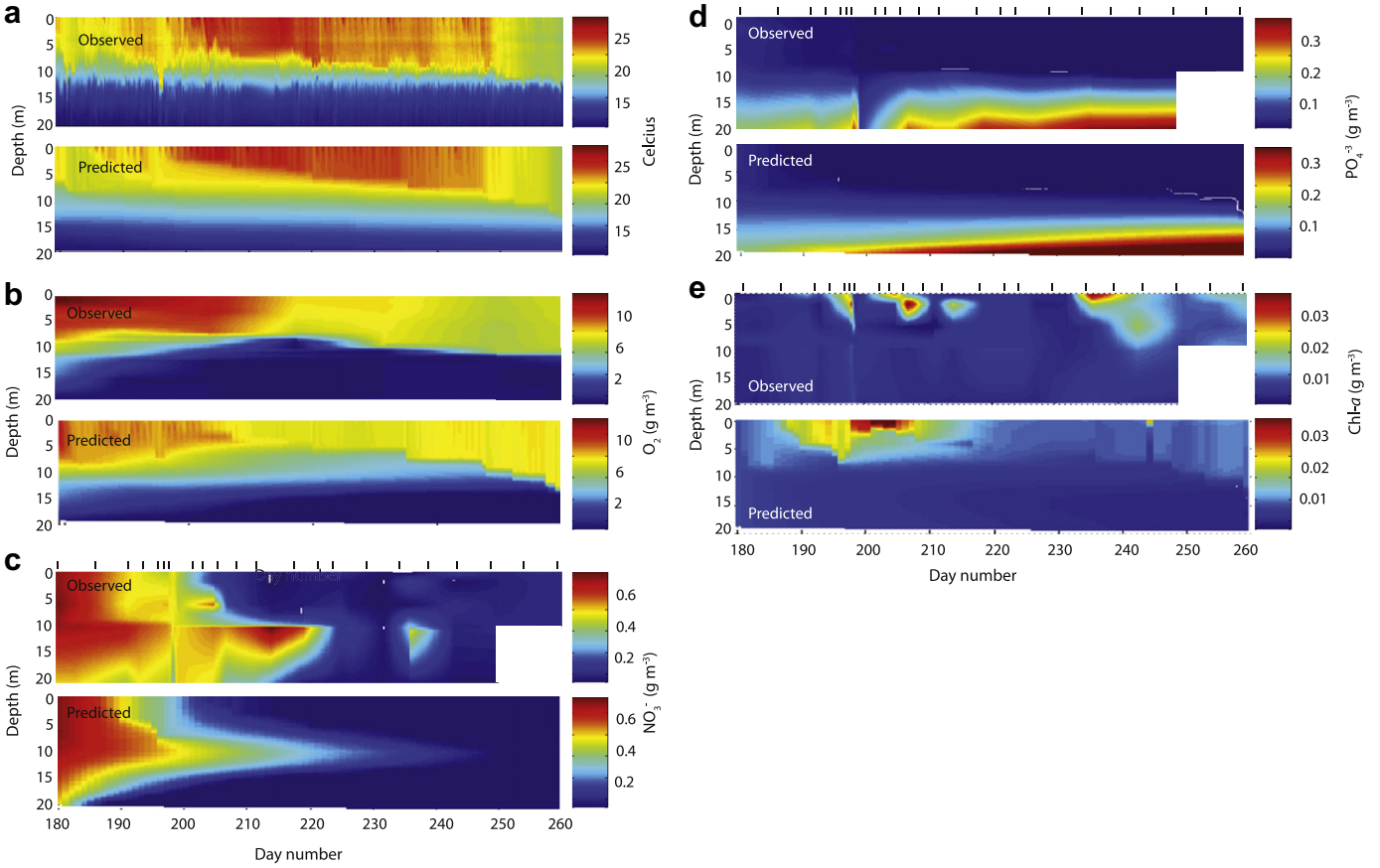

Fig. 2. Interpolated observed (upper) and predicted (lower) temperature (a), DO (b), NO_3^- (c), PO_4^{3-} (d), and chl-*a* (d). Observed temperature data (hr-1) from automated thermistor chain positioned at least every 1 m from 0 to 20 m (a), PO_4^{3-} (b), NO_3^- (c), and laboratory-extracted manual chl-*a* (d). Phosphate, NO_3^- and laboratory-extracted manual chl-*a* were sampled at 5 discrete depths from 0 to 20 m; vertical lines above observed plots c, d, and e indicate occurrence of manual sampling.

groups from the slope of this relationship (K_{eA}: 0.198 m^2 (mg chl-*a*)$^{-1}$). We assumed that the *y*-intercept (0.454 m^{-1}) of the regression line fit to the data was an estimate of K_d for all light-attenuating materials in the water column other than phytoplankton (i.e. CDOM, inorganic constituents, and pure water). We assumed the attenuation of pure water to be 0.05 m^{-1} (Pope and Fry, 1997). The remaining attenuation (0.404 m^{-1}) was attributed to CDOM. Assuming a constant relationship between CDOM and DOC, we generated a K_{eDOC} per unit DOC based on the mean DOC concentration over the study period in Lake Mendota. The resulting K_{eDOC} estimate, (0.0072 m^2 (g DOC)$^{-1}$) is within the range of literature values for DOC-specific absorbance (Morris et al., 1995).

2.4.2. Water column nitrification rate

Simulated nitrification in the water column is modeled in CAEDYM as a function of a maximum temperature-referenced (20 °C) nitrification rate (μ_{NIT}) modified by temperature, concentrations of NH_4^+ and DO, and a half saturation constant for the effect of oxygen on nitrification. To estimate the maximum nitrification rate, we applied the following relationship:

$$k_{nit} = [(\log C_2 - \log C_1)*2.303]/(T_2 - T_1) \quad (2)$$

where k_{nit} is maximum nitrification rate when oxygen is saturated in the water at the mean of the observed temperatures, T_2 and T_1, and C_n is nitrate concentration at time t_n. Nitrification rate was corrected for temperature using an Arrhenius relationship:

$$k_{nit} = k_{nit\,20} \cdot \upsilon_{chem}(T_{avg} - 20) \quad (3)$$

where $k_{nit\,20}$ is the maximum nitrification rate under oxygen saturation at 20 °C, T_{avg} is the average of temperature, *T*, at t_1 and t_2, and υ_{chem} is the temperature multiplier (1.08; Jorgensen and Bendoricchio, 2001).

After fall turnover in Lake Mendota, a near-linear increase in NO_3^- concentrations initially occurs (t_1 through t_2; approximately day 265–335 in 2008) under saturated DO conditions. The source of the increase is presumably nitrification associated with oxidation of NH_4^+ to NO_3^-, as evidenced by a simultaneous decrease in NH_4^+. The half saturation constant for nitrification dependence on DO ($k_{DO\,nit}$) was estimated by visually inspecting a plot of NO_3^- versus DO concentration and identifying a step change in NO_3^- concentration as DO approaches zero; the DO concentration at this break was identified as the half saturation constant. We investigated trends for all available years (1995–2008), and used 2008 estimates for parameter values; consistent patterns in DO, NO_3^-, and NH_4^+ were observed following fall mixis from 1995 to 2008.

2.4.3. Sediment nutrient flux

Fluxes of C, N, P, and O across the sediment-water boundary were simulated as a function of an assigned maximum rate referenced to a standard temperature (20 °C) and in turn modified by temperature, pH and DO. We estimated maximum fluxes by assuming hypolimnetic accumulation or loss of the variable of interest during summer stratification reflected sediment release or uptake, respectively. Sediment fluxes of NO_3^-, NH_4^+, PO_4^{3-}, dissolved oxygen (i.e., sediment oxygen demand; SOD), DOC, dissolved organic nitrogen (DON), and dissolved organic phosphorus (DOP) were estimated in this manner. Hypolimnetic accumulation rate constants for these nutrients were estimated during summer stratification from 1995 to 2008 as:

$$R_{chem} = (C_2 - C_1)/(t_2 - t_1) \quad (4)$$

Where R_{chem} is the maximum linear rate of hypolimnetic accumulation of the variable, calculated as the difference in concentration between C_1 and C_2 from time t_1 to t_2. The value of R_{chem} was normalized by volume to give a rate of change of concentration (g m^{-3} d^{-1}) and divided by mean hypolimnetic depth (fixed at 7.3 m from seasonally average estimates) to yield the maximum sediment flux term, S_{chem} (g m^{-2} d^{-1}). Fluxes were corrected for temperature using an Arrhenius relationship analogous to Eq. (3). Observations made at the maximum routine sampling depth (20 m) were used for this analysis, although hypolimnetic C, N, P, and O concentrations are not necessarily homogenous with depth. Rate of change for N, P, and O during summer stratification were greatest at 20 m as compared to at other depths (data not shown), and thus represent maximum possible fluxes that could be derived from observational data. This simplifying assumption ignores the effect of spatial heterogeneity in sediment flux and the influence of biomass accumulation in the deepest part of the lake, both of which could be contributing to the most extreme flux rates in the deepest part of the lake, resulting in an overestimate of the maximum potential fluxes. The half saturation constant for maximum sediment

nutrient flux dependence on DO ($S_{DO\ chem}$) was estimated by visually inspecting a plot of the concentration of the relevant nutrient species versus DO concentration during summer stratification and identifying a step change in nutrient concentration as DO approached zero as described above for rates of nitrification. We investigated all available NTL LTER data and consistent patterns of hypolimnetic nutrient accumulation were observed during summer stratification from 1995 to 2008, but we used quantitative values for 2008 to define relevant sediment flux parameter values. Observation-based estimates and literature values specific to Lake Mendota were available for sediment oxygen demand (K_{SOD}) and sediment PO_4^{3-} flux (SPO_4). However, key state variables were highly sensitive to these parameters, and thus manual manipulation to minimize error was required.

For DOC from 1995 to 2008, we found no relationship between S_{DOC} and time or S_{DOC} and DO. Lake Mendota DOC is relatively low (mean hypolimnetic DOC 5.9 g m^{-3}, standard deviation 1.1 g m^{-3}) and has little temporal or spatial variation. Based on the DOC observations, and because of absence of DOP and DON measurements, we assumed no sediment flux of DOC and that DOP and DON sediment fluxes were likewise negligible, i.e., S_{DOC}, S_{DOP}, and S_{DON} were set to zero.

2.5. Calibration

With known inflows and water elevation, the water balance was closed by estimating outflow discharge that minimized the error in observed and predicted water level. The flux of water and energy from the lake via evaporation is included in DYRESM, and this process acts to concentrate solutes in the water column. We assumed that the evaporative fluxes were properly parameterized by the wind-driven formulation in DYRESM, although we did not validate modeled evaporation rates.

Trial-and-error adjustments of sediment oxygen demand (k_{SOD}), maximum sediment flux of PO_4^{3-} (SPO_4), and phytoplankton settling velocity (v_{sA}), were made within the bounds of available published literature and system-specific field values (Table 1a) until satisfactory performance was achieved based on goodness-of-fit metrics pertaining to range and temporal pattern of DO, PO_4^{3-}, and phytoplankton biomass, respectively. These parameters were used for manual calibration because of the sensitivity of key state variables (DO, PO_4^{3-}, and phytoplankton biomass) to parameter values and because of the lack of agreement among literature and field-based values (see Table 1a for ranges from the literature and field).

2.6. Model evaluation

We used three statistical measures and wavelet analysis to evaluate model output against observational data (Table 2). Linear coefficient of determination, Spearman's rank correlation coefficient, and normalized mean absolute error were used for both manual measurements and for automated, high-frequency measurements of temperature, DO, and chl-*a* fluorescence. Wavelet analysis was used only for the high-frequency measurements of temperature, DO, and chl-*a* fluorescence, made at an instrumented platform at 0.5 m depth. Statistics were calculated for observed and predicted data at depths and times when observations were available. Observational data sampling frequency and statistical results are summarized in Table 2. All observations and predictions were compared directly, with the following exceptions: (1) all observed automated data (min^{-1}) were aggregated to hourly intervals to match the model output, (2) statistical calculations of observed chl-*a* fluorescence (RFU) and model output of chl-*a* concentration (g m^{-3}) were made after standard normal transformation of data, such that chl-*a* RFU could be evaluated directly against model output, and (3) standard normal transform preceded wavelet analysis. Water temperature measurements were interrupted periodically from July 22 through August 9 2008 (day number 204–222); only available data were considered in evaluation.

Data were compared to model output using three well-accepted goodness-of-fit measures: coefficient of determination from linear regression (R^2) values, Spearman's rank correlation coefficient (Spearman's rho), and the normalized mean absolute error (NMAE, Alewell and Manderscheid, 1998):

$$N\,MAE = \frac{\sum_t^n (|S_t - O_t|)}{n\overline{O}} \quad (5)$$

where n is number of observations, O is observed value, S is the simulated value, and t is time. NMAE provides a goodness-of-fit metric for state variables that do not cover strong gradients but whose mean values are important to reproduce. For example, epilimnetic soluble reactive phosphorus concentration can be very low during algal-dominated phases of the summer, and the observed values appear to fluctuate randomly around a low mean value quantitatively similar to analytical detection limits. In this case, it is important to reproduce the mean of the data, but not the random fluctuations, and the resultant NMAE coefficient would indicate the degree to which the mean is reproduced.

For the state variables for which high-frequency observations were available (temperature, DO, and chl-*a*), model performance was evaluated using wavelet transforms at global and individual scales (Torrence and Compo, 1998). We performed wavelet analysis on several derived metabolic variables (whole water net primary productivity, gross primary productivity and respiration) to gain insight into phytoplankton dynamics, but had no observational data with which to compare those results. Wavelet analysis was also used to assess model sensitivity to variation in three CAEDYM parameters ($K_{d\ DOC}$, SPO_4, and Min_{res}); we considered simulated variables temperature, DO, and chl-*a* concentration for this analysis. The wavelet analysis software used to generate the results presented here can be downloaded at http://atoc.colorado.edu/research/wavelets/.

Global wavelet spectra represent the sum of variability of each time scale through time and can be plotted as a power spectrum. Visualizing observation and model data as power spectra provides a convenient means for determining whether model predictions apportion variability to time scales across the entire simulation in ways consistent with the observational data. Wavelet transforms at individual scales can be used to separate data by time scale (e.g., hour, day, week periods), while maintaining the time domain. When transforms are performed on both observed and modeled data, a direct comparison of scale-specific variation can be made through time. For example, we might expect a strong diel cycle in dissolved oxygen due to metabolism at times during the summer when phytoplankton biomass is high and days are sunny. However, the dissolved oxygen signal can be driven by processes at multiple scales, such as the aforementioned metabolism and changes in solubility driven by seasonal temperature cycles. Isolating the daily scale using wavelet transforms allows us to evaluate, e.g., daily dissolved oxygen cycles without the confounding effects of other scales. Wavelet transforms have been shown to be robust to modest deviations from stationarity, i.e. constant mean and variance (Cazelles et al., 2008). Differences between the spectra of observed and modeled data may provide clues to processes missing or inappropriately represented in the model.

3. Results- evaluation of model predictions

3.1. Traditional goodness-of-fit

Surface water level at the outflow ranged 0.8 m in elevation through the simulation and was maintained within 4% of observed elevation. Water temperature and features of thermal stratification were reproduced well, including surface water temperature, metalimnetic depth, and hypolimnetic temperature (Fig. 2a). Observed and predicted temperature (T_{obs} and T_{pred}) between 0 and 20 m were highly correlated ($R^2 = 0.94$, Rho = 0.97, Table 2). The metalimnetic T_{obs} gradient was stronger than that of T_{pred}, but the observed seasonal hypolimnetic deepening by approximately 3 m was represented in the model output.

Over the duration of the simulation, the range and temporal variability of DO through the water column was well represented, though surface DO was under-predicted for most of the simulation (Fig. 2b). Under-predictions of DO at the surface (0.5 m) resulted in poorer goodness-of-fit metrics R^2 and Rho for high-frequency DO observations, but not for biweekly DO manual observations through the water column ($R^2 = 0.79$, Rho = 0.87, Table 2). NMAE metrics for both high frequency and manual DO observations against simulated DO concentrations were both low (0.26 and 0.32, respectively). The predicted oxygen gradient reflected the predicted metalimnetic thermal gradient, which was similarly weaker than the observed gradient. Statistical analyses showed that the nutrients NO_3^-, NH_4^+, PO_4^{3-}, TP, and TN were generally well represented in the simulation (Table 2), though the metalimnetic gradients were weaker than those observed (Fig. 2c and d). The model reproduced the trend of epilimnetic and hypolimnetic depletion of NO_3^- and simultaneous persistence of metalimnetic NO_3^- through ~ day 220 (Fig. 2c). A decrease in simulated epilimnetic PO_4^{3-} from 0.030 g m^{-3} to <0.005 g m^{-3} from day 180–200, and accumulation of hypolimnetic PO_4^{3-} from 0.15 g m^{-3} to 0.25 g m^{-3} over the duration of the simulation are both consistent with observed data (Fig. 2d, Table 2). Observed TN, TP, pH and DIC were significantly and positively correlated with model predictions (Table 2). Ammonium (NH_4^+) and DOC in general followed the seasonal pattern and magnitude of the observed data (Table 2). Both observed and predicted DOC had limited concentration range (~1 g m^{-3}) and no clear temporal pattern over the 90-day simulation, which resulted in poor R^2 and Spearman's rho terms, however the NMAE value was low (0.053),

Table 2
Coefficient of determination (R^2) from linear regression, Spearman's rank correlation coefficient (Spearman's rho), and NMAE value for key state variables and observed data. Number of observation indicates number of values used in analyses after outlier removal and aggregation. Depth range of 0–20 indicates discrete sampling depths detailed in methods.

State variable	Frequency of observation (aggregated frequency, when applicable)	Depth or depth range (no. of discrete depths)	Number of observations	R^2	Spearman's rho	NMAE	Wavelet analysis
Temperature	min^{-1} (hr^{-1})	0.5 (1)	1488	0.83	0.92	0.034	x
Temperature	min^{-1} (2 hr^{-1})	0–20 (24)	21,230	0.94	0.97	0.047	
DO	min^{-1} (hr^{-1})	0.5 (1)	1777	0.01	−0.04	0.26	x
DO	2 $week^{-1}$	0–20 (24)	178	0.79	0.87	0.32	
chl-*a* (in situ fluorescence)	min^{-1} (hr^{-1})	0.5(1)	1777	0.10	0.40	1	x
chl-*a* (extracted, g m^{-3})	$week^{-1}$	0–20 (5)	130	0.07	0.12	1.2	
DIC	$month^{-1}$	0–20 (11)	25	0.84	0.96	0.053	
pH	$week^{-1}$	0–20 (20)	39	0.91	093	0.020	
NH_4^+	$week^{-1}$	0–20 (5)	190	0.11	0.26	1.8	
NO_3^-	$week^{-1}$	0–20 (5)	190	0.75	0.88	0.28	
PO_4^{3-}	$week^{-1}$	0–20 (5)	189	0.33	0.39	1.6	
TN	$week^{-1}$	0–20 (5)	190	0.28	0.65	0.41	
TP	$week^{-1}$	0–20 (5)	173	0.21	0.51	0.35	
DOC	$week^{-1}$	0–20 (5)	189	0	−0.02	0.053	
A_{Aph}	2 $week^{-1}$	0–8 (integrated)	7	0.08	0.70	0.51	
A_{Mic}	2 $week^{-1}$	0–8 (integrated)	7	0.01	−0.20	0.96	
Predicted phytoplankton biomass, respiration, NPP, and GPP	n/a	n/a	2160 (for all variables)	n/a	n/a	n/a	x

reflecting the small proportion of model residuals to mean observational values.

Surface (0.5 m) and upper water column (0–8 m) chl-*a* concentration were consistently higher in the modeled data than in observed in vitro chl-*a* concentrations from day number 180–230 by ~ 0.01–0.02 g m^{-3} (Figs. 1d and 3a). Chlorophyll-*a* was over-predicted in the water column from day 0. The values of manual chl-*a* observations sometimes matched simulated chl-*a*, though shorter-term chl-*a* dynamics were not well captured, resulting in low correlation coefficients (R^2 = 0.074, Spearman's rho = 0.12). Model simulations reproduced the range of phytoplankton biomass although some temporal patterns were not reproduced (Fig. 3b and c). The *Microcystis*-like functional group (A_{Mic}) biomass increased throughout the season and was similarly simulated, though a peak in observed biomass on day 231 was not predicted (Fig. 3b). Both observed and simulated A_{Aph} biomass was lowest at the beginning and end of the simulated period, though the simulation did not predict two mid-season peaks in A_{Aph} on days 198 and 228 (Fig. 3c). Observed and simulated A_{Chlor} and A_{Diat} biomass never exceeded 1% of total phytoplankton biomass in both simulated and measured data, but were included in model configuration to represent the two additional ecologically relevant groups.

In the time domain, goodness-of-fit metrics for high-frequency (h^{-1}) observations and predictions at 0.5 m indicated good model representation of temperature (R^2 = 0.83, Rho = 0.92, and NMAE = 0.034), poorer representation of DO (R^2 = 0.01, Rho = −0.04, NMAE = 0.26), and moderate reproduction of chl-*a* concentration as compared to in situ chl-*a* fluorescence in RFU (R^2 = 0.10, Rho = 0.40, NMAE = 1).

To assess the simulated zooplankton biomass, particularly for controls on phytoplankton biomass, we consider loss of phytoplankton biomass to zooplankton grazing, which represents <1% loss of standing biomass per day. Because we model the cyanobacterial-dominated phase in Lake Mendota, we expected zooplankton grazing to be low. Observed zooplankton standing biomass ranges from 0.01 to 0.06 g C m^{-3}, which is consistent with loss of ~0.001 g C m^{-3} d^{-1} of phytoplankton biomass due to grazing. Zooplankton speciation and abundance have remained remarkably stable over the past few decades, and our simulation of small loss of phytoplankton by zooplankton grazing is consistent with historical data (Brock, 1985).

3.2. Wavelet analysis

Water temperature spectra for observations and predictions had similar pattern across scales from hours to ~25 d, with spectral peaks at the 1 d and ~13 d scales (Fig. 4a and b). Both T_{obs} and T_{pred} spectra had an increase in power at ~27 d and T_{obs} power exceeded T_{pred} at this scale. Observed DO (DO_{obs}) power spectra exceeded predicted DO (DO_{pred}) at all scales < 38 d, and both spectra had peaks at the 1 d scale, although the DO_{obs} spectra exceeded DO_{pred} spectra at that scale (Fig. 4c and d). DO_{obs} spectrum also had peaks at ~5, 13, 18, and 33 d scales; DO_{pred} spectrum had peaks of much lower power at the 7, 10, and ~17 d scales.

Wavelet analysis of chl-*a* fluorescence spectra and simulated chl-*a* concentration (after standardization of both variables) indicated higher relative power in observed chl-*a* (chl-a_{obs}) fluorescence at time scales < 10 d (Fig. 4e and f). Peaks were visible at the 3, 7, 9, and 18 d scale for chl-a_{obs} spectrum, with an average decrease in power at >18 d scale. The predicted chl-*a* (chl-a_{pred}) spectrum exhibited peaks at the 1, 5, and 13 d scales, with large increase in power especially for >20 d period.

Wavelet transforms shown for a single scale through time indicate the strength of variation at a particular frequency through time (Fig. 5). Wavelet transform at the 1 d scale for T_{obs} showed higher amplitudes than the transform for T_{pred} (Fig. 5a), but the amplitudes and phases at the 10 d scale were closely matched (Fig. 5b). The single-scale 1 d wavelet transform for DO_{obs} had higher amplitude than DO_{pred} for most of the simulated period, particularly from day 195–205 (Fig. 5c). The DO_{obs} 10 d scale had higher amplitude than DO_{pred} (Fig. 5d). The chl-a_{obs} transform had higher amplitude than chl-a_{pred} at the 1 d scale, but not at the 10 d scale (Fig. 5e and f). Observed and predicted chl-*a* transforms at the 10 d scale were out of phase through time.

Global wavelet analysis of simulated biomass, respiration, productivity, and net primary productivity (NPP) indicated strong diel signals for respiration, productivity, and NPP (Fig. 6). The biomass spectrum has low power at shorter periods and higher power with longer period. Spectra of productivity, respiration, and NPP all contain peaks at the ~12 d period, and lesser peaks at the 5–6 d period.

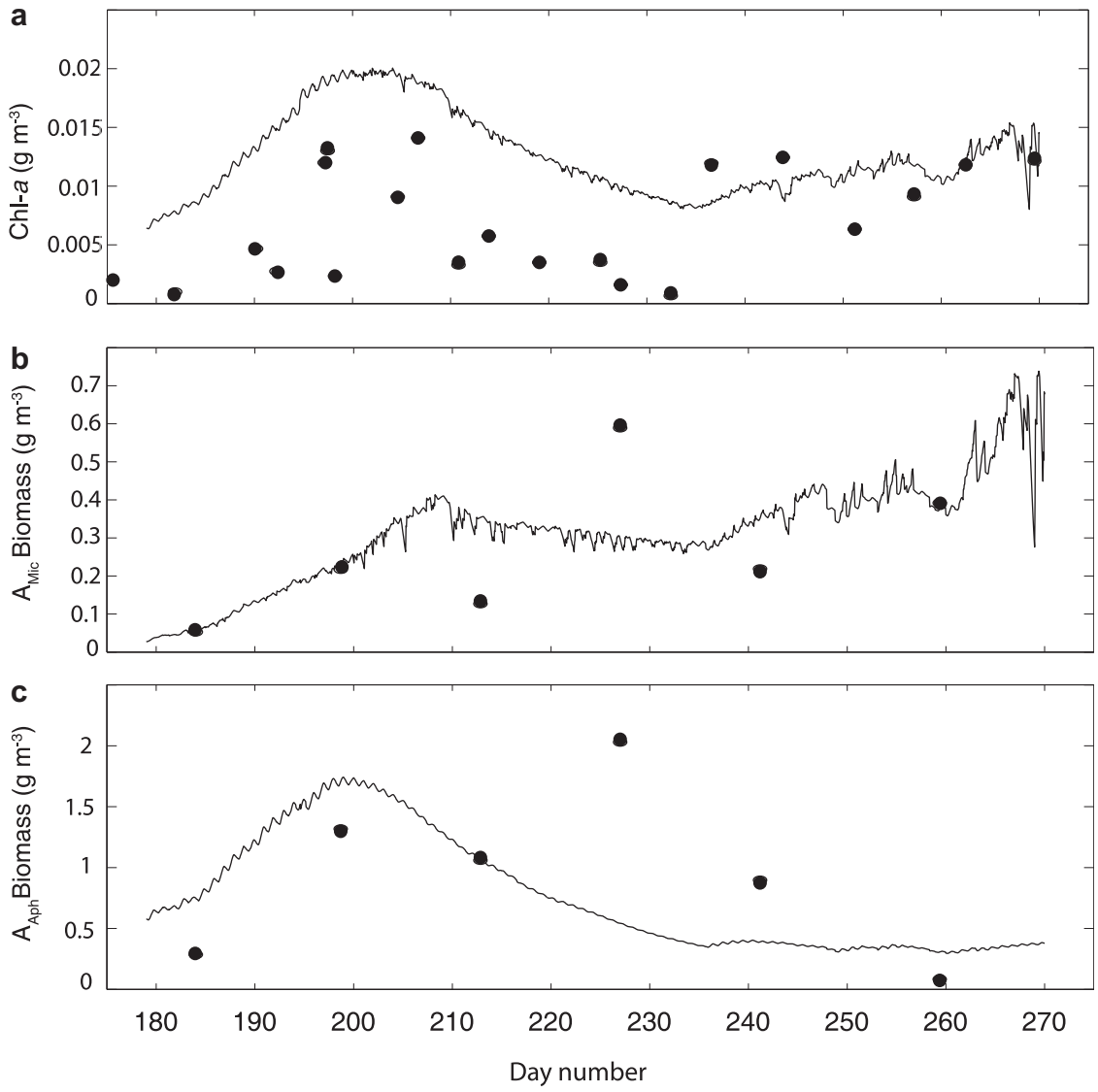

Fig. 3. Observed (solid circles) and predicted (solid line) total chlorophyll-*a* concentration (a), the Microcystis-like functional group (A_{Mic}) biomass (b) and the Aphanizomenon-like functional group (A_{Aph}) biomass (c) vertically averaged over 0–8 m depth. Predicted and observed values from 0 to 8 m vertically averaged (depth integrated) range.

4. Discussion

Aquatic ecosystem models are intended to reproduce the pattern, range, and timing of physico-chemical and biological variables driven by environmental change through time. The characteristic time scales at which environmental drivers operate (e.g. the life span of predators, the occurrence of El Niño-Southern Oscillation, or annual hydraulic flushing) have been shown to control features of aquatic ecosystems (e.g. long-term records of sedimented algal pigment, primary productivity, or water column transparency) independently at corresponding time scales, resulting in multiple scales of variation due to multiple drivers (Carpenter and Leavitt, 1991; Jassby et al., 1999, 1990). Here, we use wavelets to analyze predictions from an aquatic ecosystem model in both the time and frequency domains, assessing variability across a range of temporal scales. This allows for the more focused examination of model performance across multiple time scales, potentially highlighting missing or mischaracterized mechanisms that dominate at different time scales. To our knowledge, this represents the first work evaluating coupled hydrodynamic-water quality model prediction of dissolved oxygen and chlorophyll at short (daily to sub-day) time scales. Understanding a model's ability to reproduce variability at characteristic time scales may highlight which processes contributing to overall variability are least understood.

Wavelet analysis has been used by others to assess observed temporal variability in lakes for long-term time series (e.g. Keitt and Fischer, 2006); short-term, high-frequency data (e.g. Langman et al., 2010); and plankton spatial heterogeneity (Blukacz et al., 2009). We demonstrate that this new and complementary approach is particularly powerful when environmental modeling predictions can be compared with the ever-increasing abundance of in situ data. The use of automated sensor data for validation of numerical ecosystem model predictions has been suggested as the next step in aquatic ecosystem modeling (Arhonditsis and Brett, 2004; Beck et al., 2009), and wavelet analysis offers a methodology for using the multi-scale data in calibration and validation.

We hypothesized that variation at characteristic time scales might provide insight into important processes, both observed and modeled. Some unexpected analytical results in the frequency domain led us to discuss the implications for model setup and configuration on time-scale predictions, and motivated a closer investigation into how model parameterization affects key predictions in both the time and

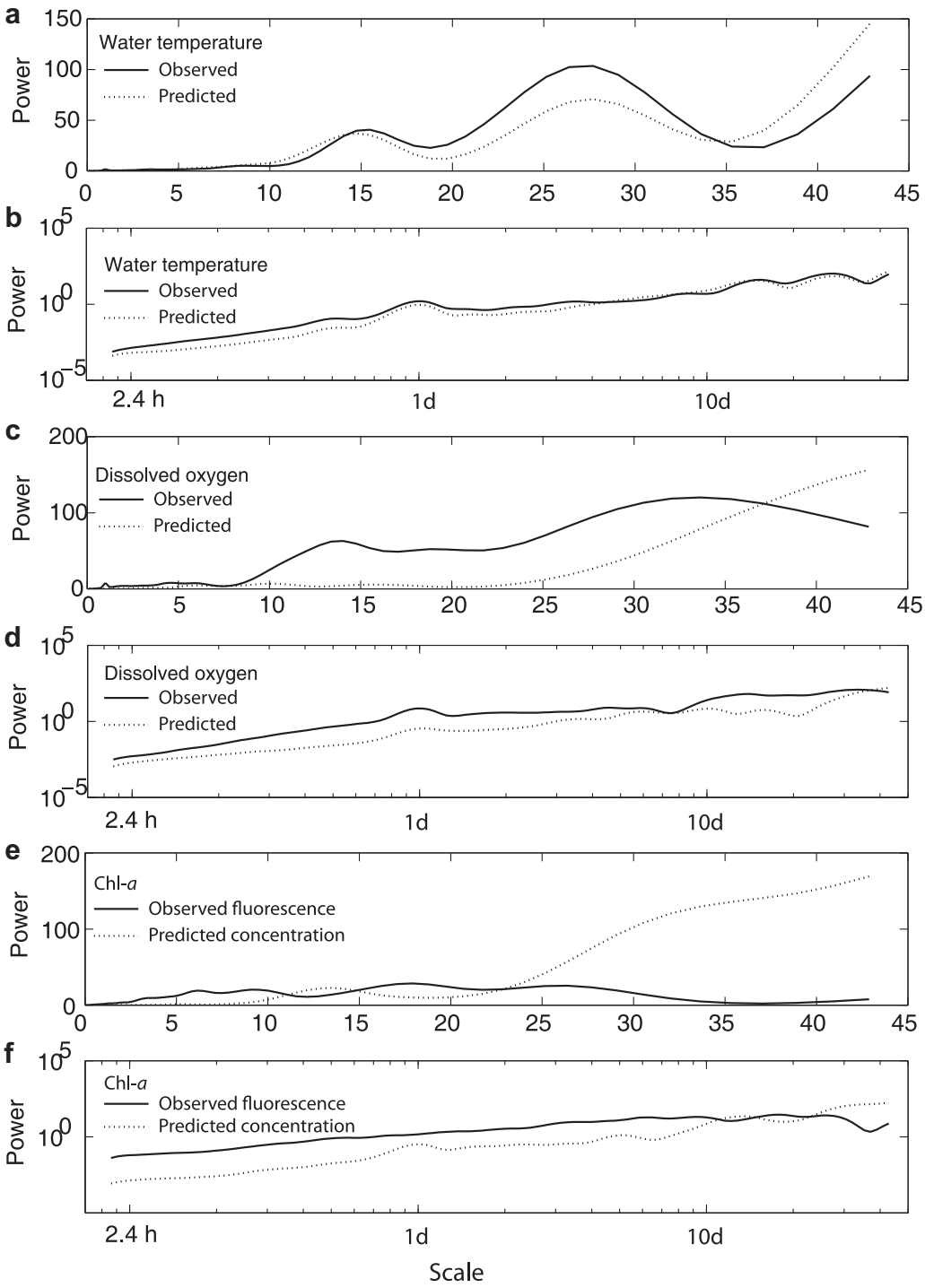

Fig. 4. Global wavelet analysis of high-frequency (hr^{-1}) temperature (a, b), dissolved oxygen (c, d) and chlorophyll-*a* (e, f) observations (black) and predictions (dashed). Global wavelet transforms are plotted on linear (a, c, and e) and logarithmic (b, d, and f) axes.

frequency domains. Finally, our particular interest in short-term phytoplankton dynamics in this study necessitated scrutiny of the well-established biomass quantification methods and newer in situ fluorometric methods, and the challenges of making meaningful use of multiple phytoplankton data streams.

4.1. Time scale prediction

The model output re-created key spectral characteristics for temperature and in part for DO, but not for chl-*a*, suggesting other factors not modeled are relevant for high-frequency variables of interest at scales of hours to weeks. We were surprised to find the observed DO and chl-*a* signals to be decoupled, but we also found the predicted metabolic variables (NPP, GPP, R) were decoupled from the predicted DO signal. In general, predicted and observed spectra for all variables converged around the 7–10 d scale, while observations had more variability than predictions at scales of hours to ~1 week (Fig. 4). It is notable that the DO_{obs} and chl-a_{obs} spectral signals were not closely coupled, particularly at lower scales around 1 d, although they are linked physiologically through metabolism. In

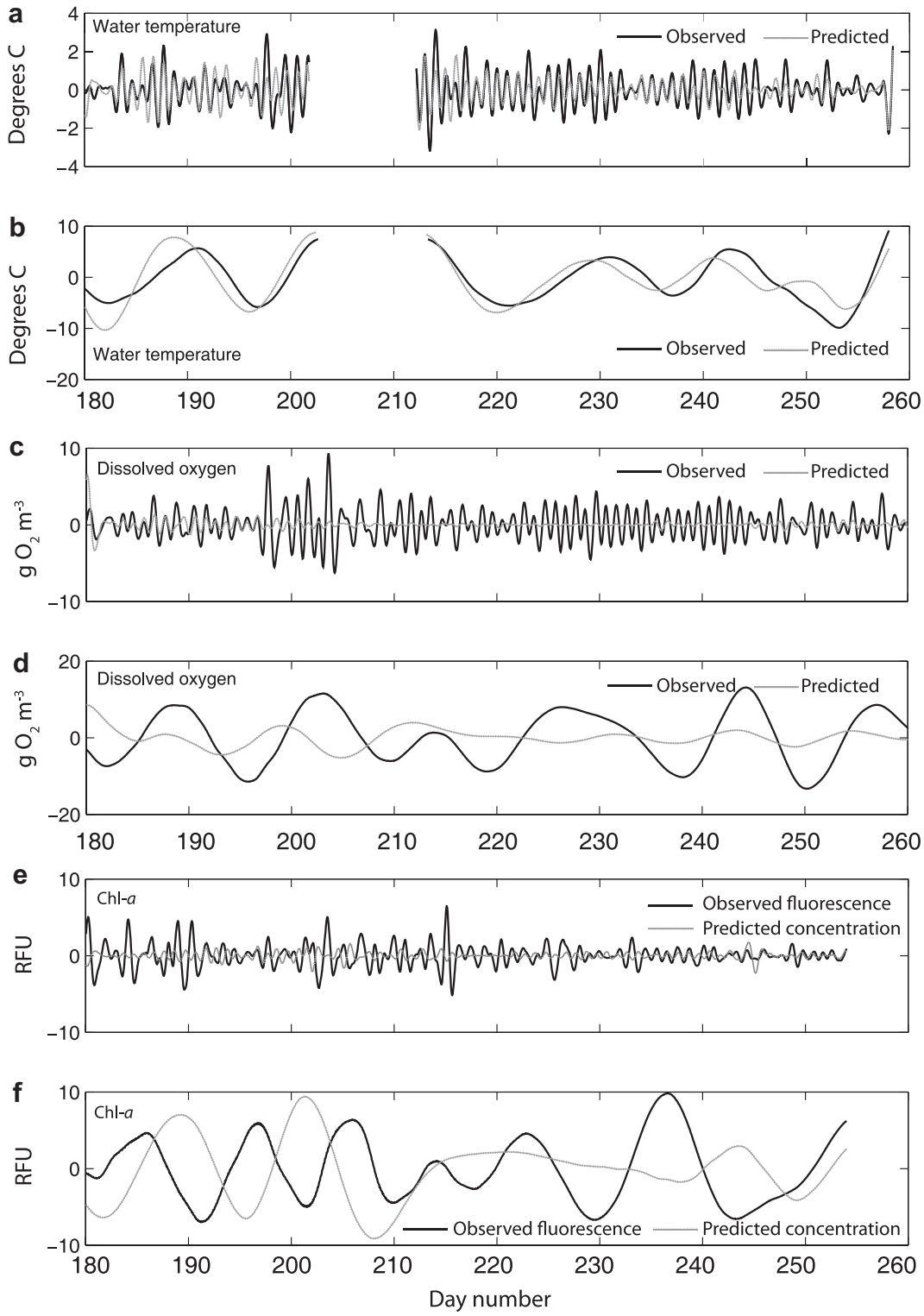

Fig. 5. Single-scale wavelet transforms of temperature (a, b), dissolved oxygen, (c, d), and chl-*a* fluorescence (e, f) at the 1 d (a, c, and f) and 10 d scale (b, d, and f). Observed data indicated with solid lines and predicted data indicated with dashed lines. Missing temperature data from day 208–218 were removed for the analysis and the two sets of adjacent data were made consecutive so that the analysis was run on a continuous time series. Single-scale transform shown here was separated after analysis to indicate missing data.

contrast, the spectra of DO_{pred} and chl-a_{pred} both had clear peaks at 7–10 d and at 1 d (Fig. 4d and f). We also expected the global spectra for the predicted productivity, respiration, and NPP for phytoplankton to exhibit similar spectral characteristics as DO_{pred} and chl-a_{pred}. However, peaks at the daily scale and at the ~10–15 d scale for these metabolic variables occurred in the chl-a_{pred} spectrum, but not in the DO_{pred} spectrum. De-coupling of closely related variables and processes in both predictions and observations in the frequency domain was unexpected and demands further investigation into drivers of variation in through time.

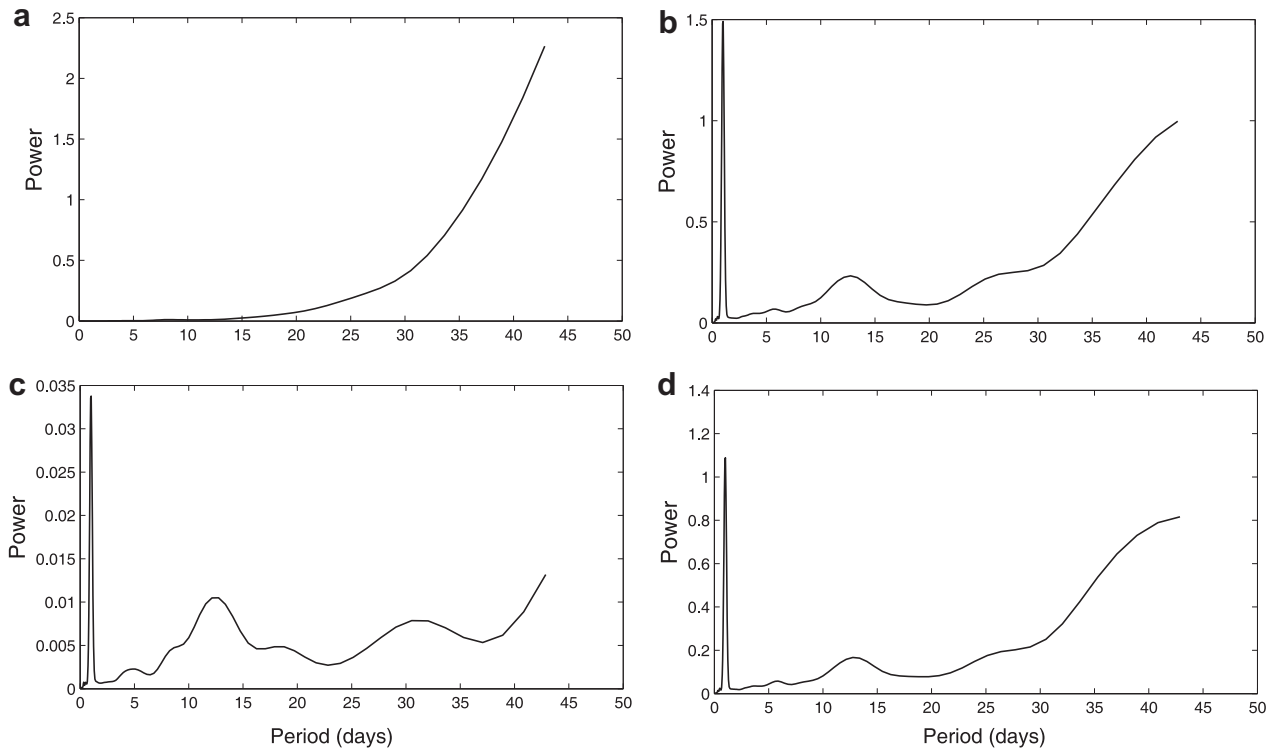

Fig. 6. Spectral analysis of biomass (a), gross primary productivity (b), respiration (c) and net primary productivity (d) for 2008 from model output.

Wavelet transform of a single scale through time demonstrates how the scale-specific timing of model predictions may not match observations. The differences in amplitude of predictions and observations for DO and chl-*a* in the single-scale wavelet transforms were especially evident in the individual scale (1 d) plots (Fig. 5). A large increase in the amplitude of the single scale DO_{obs} transform occurred from day 198–208. A similar increase in amplitude of chl-a_{obs} did not occur. The high amplitude of DO_{obs} during this period may be explained by physical changes related to a large precipitation event that occurred on day 194, where inflow volumes were approximately three times base-flow. The event resulted in observable disturbances in water temperature, DO, PO_4^{3-}, NO_3^-, (Fig. 2), and NH_4^+ and DOC (not shown) around day 198. Water column chemical gradients for PO_4^{3-}, NO_3^-, NH_4^+, and DOC were also disrupted; hypolimnetic PO_4^{3-} fell to < 100 mg m^{-3} and upper water column (0–10 m) NO_3^- increased by $\sim$100 mg m^{-3}, while lower water column (10–20 m) NO_3^- decreased by $\sim$ 100 mg m^{-3}, possibly indicating the entrainment of hypolimnetic nutrients into the epilimnion. Even though daily inflow data, which included this disturbance event, were used to drive the model, we did not see the disturbance expressed in model predictions. We speculate that three-dimensional effects in the lake system that were not represented in the 1D model may explain this discrepancy between observations and predictions.

4.2. Model limitations

Ecosystem models are simplifications of the systems they represent, and cognizance of the limitations of a model permits the user to make more informed interpretation of model behavior. Some aspects of model setup and configuration that may contribute to the prediction accuracy of short-term phytoplankton dynamics in this study are explored below, and include spatial dimensionality, time-step calculation, and representation of biological state variables.

Patterns detected by automated high-frequency observations and not reproduced in the 1D model – for example, the event beginning day 198- may represent spatial heterogeneity in the horizontal dimension (Fragoso et al., 2008; Platt et al., 1970; Steele and Henderson, 1992) or vertical dynamics not accounted for in the model (e.g. those described and modeled by Serizawa et al., 2010). Hillmer et al. (2008) established an index for validation of the 1D assumption of horizontal homogeneity of phytoplankton:

$$L = (k/\mu)^{1/2} \tag{6}$$

where L is the characteristic length scale at which phytoplankton growth is offset by diffusion, k is horizontal diffusivity and μ is the net growth rate of phytoplankton. According to this index, phytoplankton patch size will exceed lake area when $k/\mu >>$ (basin scale)^2 and a 1D assumption of homogenous phytoplankton distribution is valid. When $k/\mu <<$ (basin scale)^2, patch size will be localized and the 1D assumption violated by horizontal concentration gradients (Hillmer et al., 2008). By bracketing potential horizontal diffusivity coefficients for Lake Mendota within ranges measured in systems of comparable area (0.02–0.3 m^2 s^{-1}, Peeters et al., 1996) and assuming net growth rate of 1.0 d^{-1}, a basin scale length of 6 km (Yuan, 2007), $L^2 >> k/\mu$, and the 1D assumption is not met. Thus, the variability in high-frequency observations we detected across some temporal scales may be in part due to horizontal heterogeneity, e.g. phytoplankton patchiness due to physical, chemical, or biological heterogeneity. When three dimensions are collapsed into one, and a model is calibrated to 1D observational data, spatial heterogeneity is effectively subsumed into the mean seasonal value for the training period. As with other dynamic models, caution must be exercised when applying the calibrated parameters outside of the training period, as a new set of spatially heterogeneous conditions may subsequently be at play (Hillmer et al., 2008). Kamarainen et al. (2009) used a 3D hydrodynamic model for Lake Mendota to investigate the contribution to P loading

of hypolimnetic entrainment; for that purpose, the authors found that single-location sampling to estimate average hypolimnetic P entrainment was sufficiently similar to multi-location sampling averages. For investigating the more complex processes of nutrient advection and biological response, a 3D modeling and sensing approach (as described by Vos et al. (2003)) would provide a powerful dataset for evaluating temporal and spatial predictions of a 3D model for the Lake Mendota system, but is nevertheless outside of the scope of this paper.

Likewise, the effects of the temporal resolution used in the model should be considered. The relationship between model calculation time step and prediction accuracy across time scales is unknown and deserves further investigation, particularly for short-term variation on the order of hours to days. Here, we used 1 h driver data and investigated predicted patterns at scales as short as 3 h. However, many high frequency environmental variables are measured at scales of seconds to tens of minutes on many platforms, which could provide a convenient test for time-step effects.

Surprising differences between predicted and observed chlorophyll-*a* in the time and frequency domains motivated a closer inspection of the configuration of the biogeochemical model. Here, and typically among published studies of CAEDYM, the model was configured with static chlorophyll-*a*:C ratios (chl:C) and fixed internal C content for each phytoplankton functional group. Under this configuration, predicted water column chl-*a* concentration is derived from predicted phytoplankton biomass and varies only as a function of functional group composition of biomass and total biomass. We used the long-term NTL LTER dataset to explore the validity of a static chl:C ratio assumption for this system (Fig. 7). A range of two orders of magnitude of chl:C ratios was calculated for this system between 1999 and 2008. Predicted chl:C ratios are closer to the decadal median values than to those observed at the annual, seasonal, and daily scales. Although fixed chl:C ratios are used to derive chl-*a* concentration by the model, chl:C ratios are known to vary with cell age, across species, and with variations in temperature, nutrient, and light (Geider, 1987; Reynolds, 2006). For our simulations, chl-*a* concentration was overestimated by model output from the first day of the simulation; overestimates of chl:C ratio may explain some deviation of model fit with observations. But, had a fixed chl:C ratio been assigned to fit initial conditions of observed chl-*a*, it is likely that chl-*a* goodness-of-fit would be poor later in the simulation. Likewise, the poor correspondence of observed and predicted phytoplankton functional group biomass in units of carbon concentration could be due in part to the introduction of error and/or uncertainty in observation, introduced by the static configuration of chl:C ratios used for converting microscopic cell counts to carbon units (parameters shown in Table 1c), and the de-coupling of DO and chl-*a*. As suggested by Flynn (2005b), the use of dynamic chl:C ratios by aquatic ecosystem modelers may provide more realistic representations of chl-*a* concentrations, especially relevant to those using in situ, in vitro or in vivo chl-*a* measurements as a proxy for phytoplankton biomass, but is beyond the scope of this paper.

4.3. The challenges of multiple phytoplankton quantification methods

The challenges of mapping multiple types of observational data onto one or two state variables or derived variables in the model have been encountered by others (e.g. Rigosi et al., 2011), and requires closer consideration of the relationship between observational data, model configuration and the use of multiple types of observational data (Flynn, 2005a). We focus here on model predictions of phytoplankton biomass and chl-*a* concentration, and compare them against three types of phytoplankton observations: (1) manual taxonomic identification to estimate biomass in units of carbon concentration [g C m^{-3}] and referred to as 'biomass' hereafter; (2) in vitro laboratory solvent extraction and spectrophotometric or fluorometric analysis of chl-*a* concentration, 'in vitro chl-*a*' hereafter; and (3) in situ optical chlorophyll fluorometry, 'in situ chl-*a*' hereafter. Each method has well-documented strengths and limitations (e.g. Gregor and Marsalek, 2004; Kepner and Pratt, 1994; Marra, 1997). We consider some challenges associated with the use of multiple methods for validation data in more detail below.

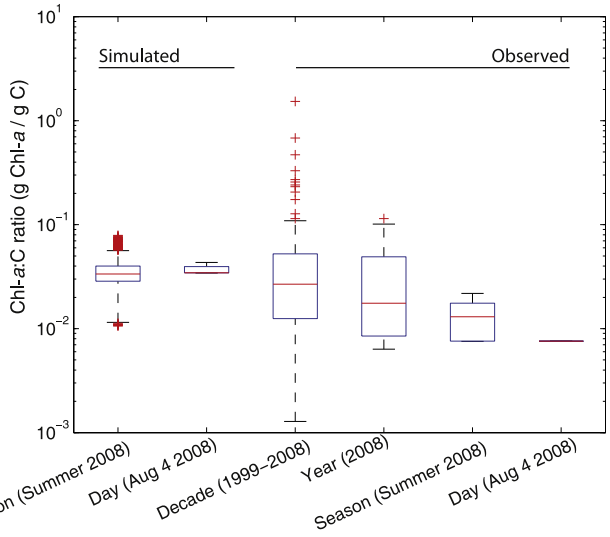

Fig. 7. Simulated and observed chlorophyll-to-carbon (Chl:C) ratios over a range of time scales. Chl:C for Aug 4 2008 is a mean of hourly values for the simulation and a single combined observation of biomass and chl-*a*.

In vitro chl-*a*, in situ chl-*a* fluorescence, and biomass estimates from microscopy are all used routinely in comparison to model predictions, and we determined how these three variables linearly correlate to one another in this system. In Lake Mendota, long-term (1995–2008) biomass and in vitro chl-*a* concentration were positively and significantly correlated ($R^2 = 0.400$, $n = 195$). The correlation coefficient between in situ chl-*a* RFU to manual in vitro chl-*a* concentration in 2008 between days 175 and 270 (where both were measured/collected at 0.5 m at the same location) was weak ($R^2 = 0.06$, $n = 17$, in situ fluorescence hourly average for the date and time corresponding to sample collection). These observations indicate that while biomass estimated from microscopy and in vitro chl-*a* concentrations are correlated, in situ chl-*a* fluorescence is not linearly correlated to in vitro chl-*a*. This is not surprising given the documented methodological limitations of chl-*a* fluorescence (e.g. Fuchs et al., 2002; Heaney, 1978). Despite these limitations, fluorescence remains as one of the only practical methods of measuring short-term variability of chl-*a*. Our results further show that in vitro chl-*a* and in situ fluorescence are not interchangeable for Lake Mendota, and the use of one or another should be intentional.

Goodness-of-fit statistics indicated that model prediction of chl-*a* concentration was better represented by in situ chl-*a* fluorescence better than in vitro solvent-extracted chl-*a* measurements (Table 2). This finding is notable because in vitro chl-*a* concentration – as an estimate of pigment concentration – is conceptually more similar to model predictions of chl-*a* concentration than in situ chl-*a* fluorescence, which is a quantification of the emission intensity (and photosystem II photochemical efficiency) of chl-*a* within cells in whole water. Deriving more meaningful units of measure for in situ chl-*a* fluorescence data requires calibration of in situ data to in lab extracted in vitro chl-*a* concentration, but would also introduce assumptions about the relationship between in vivo and in situ chl-*a* (Falkowski and Kiefer, 1985). Gregor et al. (2005) suggested that in

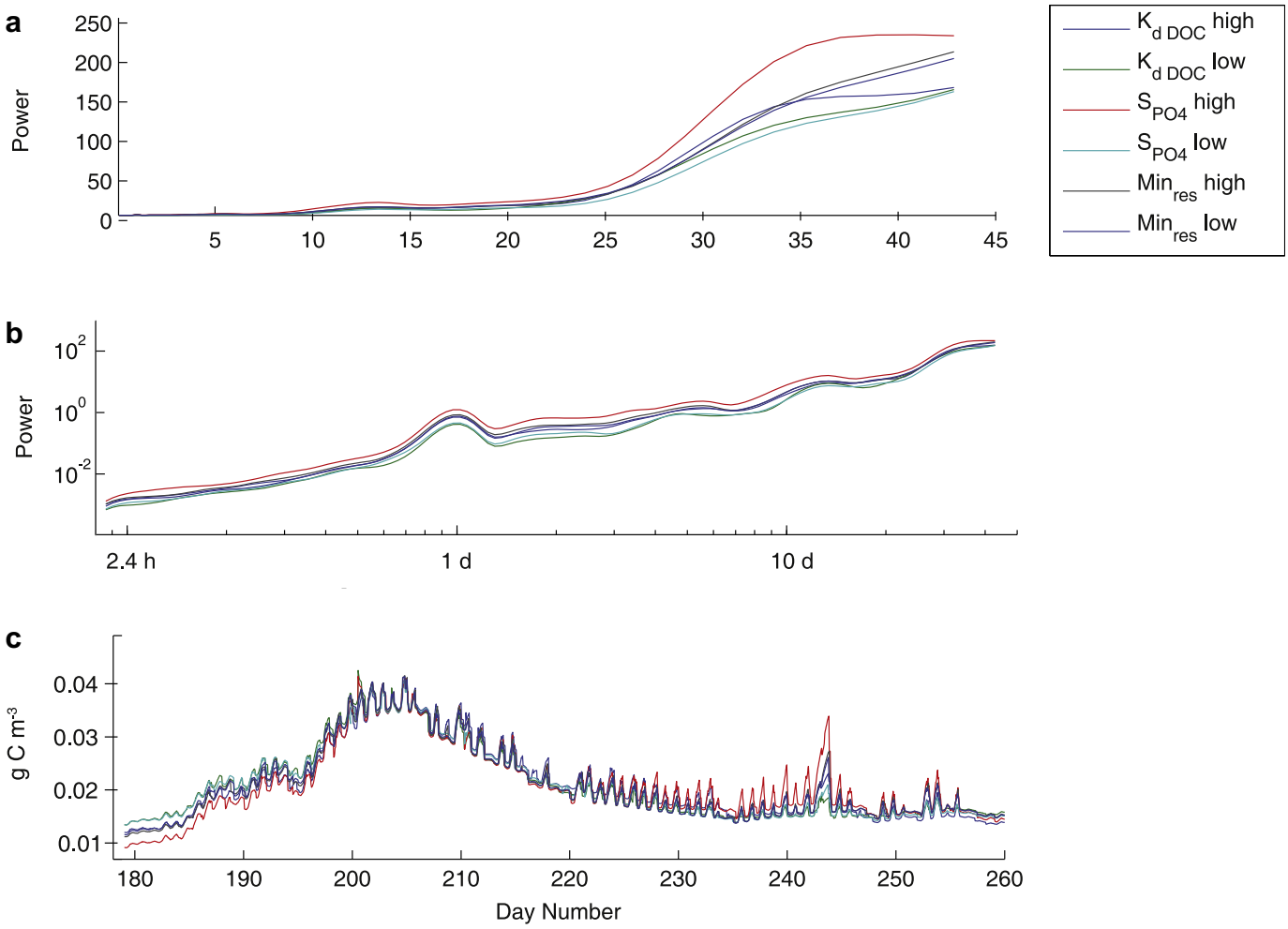

Fig. 8. The effect of modifying key CAEDYM parameters in the time and frequency domains on simulated variables temperature (a), dissolved oxygen (b), and chl-*a* (in units of g C m^{-3}) (c) as assessed by global wavelet analysis.

situ pigment fluorescence measurements should be the source of quantitative data and that taxonomic identification should be used to provide detailed taxonomic information about dominant phytoplankton taxa. In consideration of the frequency of manual sampling to inform automated data, or the use of automated high-frequency data at all, requirements for sample transport, analyst expertise, lab reagents and instruments must be balanced against the cost of sensors, platforms, and maintenance. Likewise, the optical properties of chl-*a* such as fluorescence yield, photo-adaptation and non-photochemical quenching must be acknowledged (Marra, 1997). Other types of automated sensing technologies (e.g. PHYTO-PAM, image-based monitoring and in situ flow cytometry) are being developed and in some cases are available (Shade et al., 2009), and may fill a gap in high-frequency biological data in the future.

4.4. Improving model parameterization using wavelet analysis

A few important model parameters estimated from long-term observational data led to unrealistic lake chemical predictions. Observation-based estimation of two ecologically relevant parameters was unsuitable: sediment oxygen demand (K_{SOD}) and sediment PO_4^{-3} flux (SPO_4). Both estimates from field observations were too high for model use, as they caused excessive depletion of hypolimnetic DO and buildup of hypolimnetic PO_4^{-3}. Thus, these variables were manually calibrated: the final user-defined K_{SOD} value was 0.46 g m^{-2} d^{-1}, approximately half of that estimated by Brock (1985), and only 6% of the estimate from historical hypolimnetic DO data (Table 1a). The final user-defined SPO_4 value was 0.0125 g m^{-2} d^{-1}; published laboratory estimates for SPO_4 in Lake Mendota were approximately six-fold greater than this value (Holdren and Armstrong, 1980), and three-fold greater than our estimates from historical hypolimnetic PO_4^{3-} (Table 1a). These two processes are chemically and biologically relevant in a thermally stratified eutrophic lake and the inconsistency between observed rates from laboratory experiments or estimation from field observations and final model parameter values could be due to error derived from heterogeneous hypolimnetic nutrient concentrations or biomass accumulation in hypolimnetic waters. Alternatively, these parameters may be estimated correctly, but model processes (e.g. 1D layer averaging) may be flawed.

To investigate the effects of parameterization on wavelet spectra in the frequency domain, we altered the values of three CAEDYM parameters that have strong control over key physical, chemical and biological variables. Temperature, PO_4^{3-} concentration, and phytoplankton biomass are sensitive to DOC-derived light attenuation ($K_{d\ DOC}$: standard value 0.15 g^{-1} m^3 m^{-1}, low 0.0075, high 0.03), sediment PO_4^{3-} flux (SPO_4: standard value 0.0125 g P m^{-2} d^{-1}, low 0.06, high 0.025), and Min_{res}, the minimum biomass below which zooplankton do not graze (standard value 0.01 g C m^{-3}, low 0.0, high 1.0), respectively. Model output for temperature and DO were robust to changes in values (data not shown), but mean values of chl-*a* concentration was sensitive to a range of parameters tested

(Fig. 8). The sediment PO_4^{-3} flux term had the strongest effect on chl-*a* of the three parameters tested here, likely due to the limitation of phytoplankton growth by dissolved inorganic P. This observable relationship between parameter scaling and mean seasonal values in the prediction makes calibration of the model to long simulations of years to decades tractable. However, reproducing temporal dynamics, both in terms of the timing of critical peaks (e.g., phytoplankton blooms) and the sub-seasonal cycles of the ecosystem is much more challenging. For phytoplankton biomass, patterns of variation in the frequency domain did not respond substantially to parameter optimization (Fig. 8a and b), in contrast to the average seasonal value, which was more sensitive to parameters values (Fig. 8c). The frequency response may be a result of the configured model complexity (e.g., number of trophic levels used) or the design of the model (e.g., functional forms of the fluxes). For the sensitivity analysis of these three parameters, our preliminary results indicate differential response of state variables in the time versus frequency domains; wavelet analysis could be a tool complementary for calibration techniques such as those described by Makler-Pick et al. (2011) or Rigosi et al. (2011).

5. Conclusion

We used high-frequency water quality data to assess the prediction accuracy of an aquatic numerical model over multiple temporal scales using wavelet analysis. Traditional goodness-of-fit metrics indicated physical predictions were more accurate than chemical and biological variable predictions. Wavelet analysis confirmed these findings in the frequency domain and added information about the scales at which patterns were reproduced. Physical predictions were more accurate at all scales assessed, while chemical and biological patterns were reproduced over a smaller range of scales. Wavelet analysis of in situ data is particularly relevant for the assessment of short-term predictions such as phytoplankton bloom events, and represents a new domain within which numerical models can be calibrated and validated.

Consideration of spatial heterogeneity is important for interpretation of biological observations and predictions in this system and deserves further study. There are physical–chemical–biological interactions likely not well represented in our model, and identifying what these are and how they operate at the ecosystem scale over scales of hours to weeks is critical, especially when trying to reproduce ecosystem frequency response. Investigation of how variance scales with mean values of temperature, dissolved oxygen, pigment fluorescence, and other high-frequency variables measured by automated sensing platforms would increase understanding of model and system behavior and aid interpretation of results. A better understanding of automated sensing of biological variables and their relationship to model output will improve the utility of aquatic ecosystem models. Further research is required to understand how model complexity and predictive capability interact with the type and frequency of observed variables.

Our work highlights the challenges of reconciling multiple observational methods (e.g. phytoplankton biomass and various estimates of chlorophyll as a proxy for biomass) and we show that results and subsequent interpretation may not be independent of commonly used methods. These differences reveal the need for a better understanding of how and why various methods diverge, and what useful information can be drawn from them.

Using data from sensor networks gave us a unique opportunity to evaluate the model at highly resolved time scales. For the aquatic modeling community, high-frequency sensing represents a step change for observational datasets with which to use for calibration and validation of aquatic ecological simulations. Most aquatic modelers use daily or sub-daily calculations, but predictions are usually presented at the frequency of observational data. The observational and analytical framework presented here sets the stage for future work that will doubtless include more high-frequency sensing data and, by necessity, involve a closer inspection of model behavior at high frequencies. Closer inspection will reveal surprises (e.g. the de-coupling of dissolved oxygen and primary productivity presented in this work), but we believe learning more about model behavior at all temporal scales of interest will advance the science of aquatic ecosystem simulations. Wavelet analysis allowed us to enter a new domain- frequency, leading to insight into the relationships between observations and model predictions. Now that such data are becoming more readily available, we anticipate new discovery of ecosystem processes that not only informs model development but also improves our prediction at scales pertinent to those of phytoplankton dynamics in eutrophic systems.

Acknowledgments

This work was funded in part by grants from the US National Science Foundation to the Global Lake Ecological Observatory Network (GLEON). ELK and KDM were supported by an NSF CAREER award (CBET 0738039) and the National Institute of Food and Agriculture, United States Department of Agriculture (ID number WIS01516). KCR was supported by a the EARS IGERT program, NSF DGE IGERT #0903560. This material is based upon NTL LTER work supported by the National Science Foundation under Cooperative Agreement #0822700. Wavelet software was provided by C. Torrence and G. Compo, and is available at URL: http://atoc.colorado.edu/research/wavelets/. We are grateful for the thoughtful comments of four anonymous reviewers.

References

Alewell, C., Manderscheid, B., 1998. Use of objective criteria for the assessment of biogeochemical ecosystem models. Ecological Modelling 107 (2–3), 213–224.
Alexander, R., Imberger, J., 2009. Spatial distribution of motile phytoplankton in a stratified reservoir: the physical controls on patch formation. Journal of Plankton Research 31 (1), 101–118.
Andersen, T., Hessen, D.O., 1991. Carbon, nitrogen and phosphorus content of freshwater zooplankton. Limnology and Oceanography 36 (4), 807–814.
Arhonditsis, G.B., Brett, M.T., 2004. Evaluation of the current state of mechanistic aquatic biogeochemical modeling. Marine Ecology-Progress Series 271, 13–26.
Arhonditsis, G.B., Brett, M.T., 2005a. Eutrophication model for Lake Washington (USA) Part I. Model description and sensitivity analysis. Ecological Modelling 187 (2–3), 140–178.
Arhonditsis, G.B., Brett, M.T., 2005b. Eutrophication model for Lake Washington (USA) Part II – model calibration and system dynamics analysis. Ecological Modelling 187 (2–3), 179–200.
Beck, M.B., Gupta, H., Rastetter, E., Shoemaker, C., Tarboton, D., Butler, D., Edelson, D., Graber, H., Gross, L., Harmon, T., McLaughlin, D., Paola, C., Peters, D., Scavia, D., Schnoor, J.L., Weber, L., 2009. Grand Challenges of the Future for Environmental Modeling. Warnell School of Forestry and Natural Resources. University of Georgia, Arlington, VA.
Beckel, A.L., 1987. Breaking New Waters: A Century of Limnology at the University of Wisconsin, Transaction of the Wisconsin Academy of Sciences, Arts, and Letters. Madison, WI.
Bertilsson, J., Berzins, B., Pejler, B., 1995. The occurrence of limnic microcrustaceans in relation to temperature and oxygen. Hydrobiologia 299 (2), 163–167.
Birge, E.A., 1915. The Heat Budgets of American and European Lakes. In: Transaction of the Wisconsin Academy of Sciences, Arts, and Letters, Madison, WI, pp. 116–213.
Birge, E.A., Juday, C., 1911. The Inland Lakes of Wisconsin: The Dissolved Gases of the Water and Their Biological Significance. Wisconsin Geological and Natural History Survey Bulletin 22 Scientific Series No. 7. Madison, WI.
Blukacz, E.A., Shuter, B.J., Sprules, W.G., 2009. Towards understanding the relationship between wind conditions and plankton patchiness. Limnology and Oceanography 54 (5), 1530–1540.
Brock, T.D., 1985. A Eutrophic Lake, Lake Mendota, WI, first ed. Springer-Verlag, New York.
Butler, J.N., 1982. Carbon Dioxide Equilibria and Their Applications. Addison-Wesley.
Butterwick, C., Heaney, S.I., Talling, J.F., 2005. Diversity in the influence of temperature on the growth rates of freshwater algae, and its ecological relevance. Freshwater Biology 50 (2), 291–300.

Carmichael, W.W., 2002. Health effects of toxin producing cyanobacteria: "The Cyanohabs". In: Melchiorre, S., Viaggiu, E., Bruno, M. (Eds.), Freshwater Harmful Algal Blooms: Health Risk and Control Management. Istituto Superiore di Sanità Istituto Superiore di Sanità, Rome, Italy, pp. 70–80.
Carpenter, S.R., Lathrop, R.C., Nowak, P., Bennett, E.M., Reed, T., Soranno, P.A., 2006. The Ongoing Experiment: Restoration of Lake Mendota and Its Watershed. Oxford University Press.
Carpenter, S.R., Leavitt, P.R., 1991. Temporal variation in a paleolimnological record arising from a trophic Cascade. Ecology 72 (1), 277–285.
Cazelles, B., Chavez, M., Berteaux, D., Menard, F., Vik, J.O., Jenouvrier, S., Stenseth, N.C., 2008. Wavelet analysis of ecological time series. Oecologia 156 (2), 287–304.
Culver, D.A., Boucherle, M.M., Bean, D.J., Fletcher, J.W., 1985. Biomass of freshwater crustacean zooplankton from length–weight regressions. Canadian Journal of Fisheries and Aquatic Sciences 42 (8), 1380–1390.
Degobbis, D., Gilmartin, M., 1990. Nitrogen, phosphorus, and biogenic silicon budgets for the northern Adriatic Sea. Oceanologica Acta 13 (1), 31–45.
Demott, W.R., 1982. Feeding selectivities and relative ingestion rates of Daphnia and Bosmina. Limnology and Oceanography 27 (3), 518–527.
Dobberfuhl, D.R., Elser, J.J., 2000. Elemental stoichiometry of lower food web components in arctic and temperate lakes. Journal of Plankton Research 22 (7), 1341–1354.
Dugdale, V.A., Dugdale, R.C., 1962. Nitrogen metabolism in lakes. II. role of nitrogen fixation in sanctuary Lake Pennsylvania. Limnology and Oceanography 7 (2), 170–177.
Elliott, J.A., Persson, I., Thackeray, S.J., Blenckner, T., 2007. Phytoplankton modelling of Lake Erken, Sweden by linking the models PROBE and PROTECH. Ecological Modelling 202 (3–4), 421–426.
Falkowski, P., Kiefer, D.A., 1985. Chlorophyll-a fluorescence in phytoplankton – relationship to photosynthesis and biomass. Journal of Plankton Research 7 (5), 715–731.
Flynn, K.J., 2005a. Castles built on sand: dysfunctionality in plankton models and the inadequacy of dialogue between biologists and modellers. Journal of Plankton Research 27 (12), 1205–1210.
Flynn, K.J., 2005b. Modelling marine phytoplankton growth under eutrophic conditions. Journal of Sea Research 54 (1), 92–103.
Fogg, G.E., 1949. Growth and heterocycst production in Anabena cylindrica Lemm II. in relation to carbon and nitrogen metabolism. Annals of Botany London 13, 241–259.
Foy, R.H., Gibson, C.E., Smith, R.V., 1976. The influence of daylength, light intensity, and temperature on the growth rates of planktonic blue-green algae. British Phycological Journal 11 (2), 151–163.
Fragoso, C.R., Marques, D., Collischonn, W., Tucci, C.E.M., van Nes, E.H., 2008. Modelling spatial heterogeneity of phytoplankton in Lake Mangueira, a large shallow subtropical lake in South Brazil. Ecological Modelling 219 (1–2), 125–137.
Fuchs, E., Zimmerman, R.C., Jaffe, J.S., 2002. The effect of elevated levels of phaeophytin in natural water on variable fluorescence measured from phytoplankton. Journal of Plankton Research 24 (11), 1221–1229.
Gal, G., Hipsey, M.R., Parparov, A., Wagner, U., Makler, V., Zohary, T., 2009. Implementation of ecological modeling as an effective management and investigation tool: Lake Kinneret as a case study. Ecological Modelling 220 (13–14), 1697–1718.
Galkovskaja, G.A., 1987. Planktonic rotifers and temperature. Hydrobiologia 147, 307–317.
Geider, R.J., 1987. Light and temperature dependence of the carbon to chlorophyll-a ratio in microalgae and cyanobacteria – implications for physiology and growth of phytoplankton. New Phytologist 106 (1), 1–34.
Gophen, M., 1976a. Temperature effect on lifespan, metabolism, and development time of *Mesocyclops-leuckarti*. Oecologia 25 (3), 271–277.
Gophen, M., 1976b. Temperature-dependence of food-intake, ammonia excretion and respiration in *Ceriodaphnia-reticulata* (Lake Kinneret, Israel). Freshwater Biology 6 (5), 451–455.
Gophen, M., Azoulay, B., 2002. The trophic status of zooplankton communities in Lake Kinneret (Israel). Verhandlungen des Internationalen Verein Limnologie 28, 836–839.
Gregor, J., Geris, R., Marsalek, B., Hetesa, J., Marvan, P., 2005. In situ quantification of phytoplankton in reservoirs using a submersible spectrofluorometer. Hydrobiologia 548, 141–151.
Gregor, J., Marsalek, B., 2004. Freshwater phytoplankton quantification by chlorophyll alpha: a comparative study of in vitro, in vivo and in situ methods. Water Research 38 (3), 517–522.
Hadas, O., Malinsky-Rushansky, N., Pinkas, R., Cappenberg, T.E., 1998. Grazing on autotrophic and heterotrophic picoplankton by ciliates isolated from Lake Kinneret, Israel. Journal of Plankton Research 20 (8), 1435–1448.
Hamels, I., Mussche, H., Sabbe, K., Muylaert, K., Vyverman, W., 2004. Evidence for constant and highly specific active food selection by benthic ciliates in mixed diatoms assemblages. Limnology and Oceanography 49 (1), 58–68.
Haney, J., Trout, M., 1985. Size selective grazing by zooplankton in Lake Titicaca. Archiv fuer Hydrobiologie (21), 147–160.
Hanson, P.C., Carpenter, S.R., Armstrong, D.E., Stanley, E.H., Kratz, T.K., 2006. Lake dissolved inorganic carbon and dissolved oxygen: changing drivers from days to decades. Ecological Monographs 76 (3), 343–363.
Harris, G.P., 1987. Time-series analysis of water-quality data from Lake Ontario – implications for the measurement of water-quality in large and small lakes. Freshwater Biology 18 (3), 389–403.
Healey, F.P., Hendzel, L.L., 1979. Indicators of phosphorus and nitrogen deficiency in 5 algae in cultures. Journal of the Fisheries Research Board of Canada 36 (11), 1364–1369.
Heaney, S.I., 1978. Some observations on the use of the in vivo fluorescence technique to determine chlorophyll-a in natural populations and cultures of freshwater phytoplankton. Freshwater Biology 8 (2), 115–126.
Hillmer, I., van Reenen, P., Imberger, J., Zohary, T., 2008. Phytoplankton patchiness and their role in the modelled productivity of a large, seasonally stratified lake. Ecological Modelling 218 (1–2), 49–59.
ss Hipsey et al., Should be Hipsey, M. R., unpublished.
Holdren, G.C., Armstrong, D.E., 1980. Factors affecting phosphorus release from intact lake sediment cores. Environmental Science & Technology 14 (1), 79–87.
Imai, H., Chang, K.H., Kusaba, M., Nakano, S., 2009. Temperature-dependent dominance of microcystis (Cyanophyceae) species: *M. aeruginosa* and *M. wesenbergii*. Journal of Plankton Research 31 (2), 171–178.
Imberger, J., Patterson, J.C., 1981. A dynamic reservoir simulation model- DYRESM 5. In: Fischer, H.B. (Ed.), Transport Models for Inland and Coastal Waters. Academic Press, New York.
Janse, J.H., Scheffer, M., Lijklema, L., Van Liere, L., Sloot, J.S., Mooij, W.M., 2010. Estimating the critical phosphorus loading of shallow lakes with the ecosystem model PCLake: sensitivity, calibration and uncertainty. Ecological Modelling 221 (4), 654–665.
Jassby, A.D., Goldman, C.R., Reuter, J.E., Richards, R.C., 1999. Origins and scale dependence of temporal variability in the transparency of Lake Tahoe, California-Nevada. Limnology and Oceanography 44 (2), 282–294.
Jassby, A.D., Powell, T.M., Goldman, C.R., 1990. Interannual fluctuations in primary production: direct physical effects and the trophic cascade at Castle Lake, California. Limnology and Oceanography 35 (5), 1021–1038.
Jensen, T.C., Verschoor, A.M., 2004. Effects of food quality on life history of the rotifer Brachionus calyciflorus Pallas. Freshwater Biology 49 (9), 1138–1151.
Jonasson, S., Eriksson, J., Berntzon, L., Spacil, Z., Ilag, L.L., Ronnevi, L.O., Rasmussen, U., Bergman, B., 2010. Transfer of a cyanobacterial neurotoxin within a temperate aquatic ecosystem suggests pathways for human exposure. Proceedings of the National Academy of Sciences of the United States of America 107 (20), 9252–9257.
Jorgensen, S.E., Bendoricchio, G., 2001. Fundamentals of Ecological Modelling, third ed. Elsevier Science Oxford, UK.
Juday, C., 1914. The Inland Waters of Wisconsin: The Hydrography and Morphometry of the Lakes. Wisconsin Geological and Natural History Survey Bulletin 27 Scientific Series No. 9. Madison, WI.
Kamarainen, A.M., Yuan, H.L., Wu, C.H., Carpenter, S.R., 2009. Estimates of phosphorus entrainment in Lake Mendota: a comparison of one-dimensional and three-dimensional approaches. Limnology and Oceanography-Methods 7, 553–567.
Keitt, T.H., Fischer, J., 2006. Detection of scale-specific community dynamics using wavelets. Ecology 87 (11), 2895–2904.
Kepner, R.L., Pratt, J.R., 1994. Use of fluorochromes for direct enumeration of total bacteria in environmental-samples – past and present. Microbiological Reviews 58 (4), 603–615.
Kirk, J.T.O., 1994. Estimation of the absorption and the scattering coefficients of natural waters by use of underwater irradiance measurements. Applied Optics 33 (15), 3276–3278.
Koltun, G.F., Eberle, M., Gray, J.R., Glysson, G.D., 2006. User's manual for the graphical constituent loading analysis system (GCLAS). In: U.T.a. (Ed.), Methods, p. 51.
Lampert, W., 1974. Method for determining food selection by zooplankton. Limnology and Oceanography 19 (6), 995–998.
Lampert, W., 1986. Response of the respiratory rate of Daphnia-magna to changing food conditions. Oecologia 70 (4), 495–501.
Lampert, W., 2007. Limnoecology. Oxford University Press Inc.
Landry, M., Hassett, R., 1985. Time scales in behavioral, biochemical, and energetic adaptations to food-limiting conditions. Archiv fur Hydrobiologie (21), 209–211.
Langman, O.C., Hanson, P.C., Carpenter, S.R., Hu, Y.H., 2010. Control of dissolved oxygen in northern temperate lakes over scales ranging from minutes to days. Aquatic Biology 9 (2), 193–202.
Lathrop, R.C., 1979. Dane County water quality plan. In: D.C.R.P. (Ed.), Commission. Madison, WI.
Lathrop, R.C., Carpenter, S.R., Robertson, D.M., 1999. Summer water clarity responses to phosphorus, *Daphnia* grazing, and internal mixing in Lake Mendota. Limnology and Oceanography 44 (1), 137–146.
Lean, D.R.S., 1973a. Movements of phosphorus between its biologically important forms in lake water. Journal of the Fisheries Research Board of Canada 30 (10), 1525–1536.
Lean, D.R.S., 1973b. Phosphorus dynamics in lake water. Science 179 (4074), 678–680.
Lovell, C.R., Konopka, A., 1985. The effects of temperature on bacterial production in a dimictic eutrophic lake. FEMS Microbiology Ecology 31 (3), 135–140.
Madoni, P., Berman, T., Hadas, O., Pinkas, R., 1990. Food selection and growth of the planktonic ciliate *Coleps-hirtus* isolated from a monomictic subtropical lake. Journal of Plankton Research 12 (4), 735–741.
Magnuson, J.J., Kratz, T.K., Benson, B.J., 2006. The challenge of time and space in ecology. In: Magnuson, J.J., Kratz, T.K., Benson, B.J. (Eds.), Long-term Dynamics of Lakes in the Landscape: Long-term Ecological Research on North Temperate Lakes. Oxford University Press, pp. 3–16.
Makino, W., Cotner, J.B., 2004. Elemental stoichiometry of a heterotrophic bacterial community in a freshwater lake: implications for growth- and resource-dependent variations. Aquatic Microbial Ecology 34 (1), 33–41.
Makler-Pick, V., Gal, G., Gorfine, M., Hipsey, M.R., Carmel, Y., 2011. Sensitivity analysis for complex ecological models – a new approach. Environmental Modelling & Software 26 (2), 124–134.

Markensten, H., Moore, K., Persson, I., 2010. Simulated lake phytoplankton composition shifts toward cyanobacteria dominance in a future warmer climate. Ecological Applications 20 (3), 752–767.
Marra, J., 1997. Analysis of diel variability in chlorophyll fluorescence. Journal of Marine Research 55 (4), 767–784.
McCauley, E., 1984. A Manual on Methods for the Assessment of Secondary Production in Fresh Waters. Blackwell Sci. Publ., Oxford.
Morris, D.P., Zagarese, H., Williamson, C.E., Balseiro, E.G., Hargreaves, B.R., Modenutti, B., Moeller, R., Queimalinos, C., 1995. The attentuation of solar UV radiation in lakes and the role of dissolved organic carbon. Limnology and Oceanography 40 (8), 1381–1391.
NTL-LTER, 2011a. Biological Dataset. Madison, WI.
NTL-LTER, 2011b. Chemical Limnology Dataset. In: North Temperate Lakes Long Term Ecological Research Program. Madison, WI. http://www.lternet.edu/sites/ntl/.
NTL-LTER, 2011c. Physical Limnology Dataset. In: North Temperate Lakes Long Term Ecological Research Program. Madison, WI. http://www.lternet.edu/sites/ntl/.
Peeters, F., Wuest, A., Piepke, G., Imboden, D.M., 1996. Horizontal mixing in lakes. Journal of Geophysical Research-Oceans 101 (C8), 18361–18375.
Platt, T., Dickie, L.M., Trites, R.W., 1970. Spatial heterogeneity of phytoplankton in a nearshore environment. Journal of the Fisheries Research Board of Canada 27 (8), 1453–1473.
Pollingher, U., Berman, T., 1982. Relative contributions of net and nanno phytoplankton to primary production in Lake Kinneret (Israel). Archiv fur Hydrobiologie 96 (1), 33–46.
Pope, R.M., Fry, E.S., 1997. Absorption spectrum (380–700 nm) of pure water .2. Integrating cavity measurements. Applied Optics 36 (33), 8710–8723.
Porter, J.H., Nagy, E., Kratz, T.K., Hanson, P., Collins, S.L., Arzberger, P., 2009. New eyes on the world: advanced sensors for ecology. Bioscience 59 (5), 385–397.
Reynolds, C., 2006. The Ecology of Phytoplankton, third ed. Cambridge University Press, New York.
Rigosi, A., MarcÈ, R., Escot, C., Rueda, F.J., 2011. A calibration strategy for dynamic succession models including several phytoplankton groups. Environmental Modelling & Software 26 (6), 697–710.
Robson, B.J., Hamilton, D.P., 2004. Three-dimensional modelling of a microcystis bloom event in the Swan River estuary, Western Australia. Ecological Modelling 174 (1–2), 203–222.
Romero, J.R., Antenucci, J.P., Imberger, J., 2004. One- and three-dimensional biogeochemical simulations of two differing reservoirs. Ecological Modelling 174 (1–2), 143–160.
Sandgren, 1995. Chrysophyte Algae: Ecology, Phylogeny, and Development. Cambridge University Press.
Sandgren, C., 1988. Growth and Reproductive Strategies of Freshwater Phytoplankton. Cambridge University Press.
Scavia, D., Lang, G.A., Kitchell, J.F., 1988. Dynamics of Lake Michigan plankton – a model evaluation of nutrient loading, competition, and predation. Canadian Journal of Fisheries and Aquatic Sciences 45 (1), 165–177.
Serizawa, H., Amemiya, T., Itoh, K., 2010. Effects of buoyancy, transparency and zooplankton feeding on surface maxima and deep maxima: comprehensive mathematical model for vertical distribution in cyanobacterial biomass. Ecological Modelling 221 (17), 2028–2037.
Serruya, C., Edelstein, M., Pollingher, U., Serruya, S., 1974. Lake Kinneret sediments: nutrient composition of the pore water and mud water exchanges. Limnology and Oceanography 19 (3), 489–508.
Shade, A., Carey, C.C., Kara, E., Bertilsson, S., McMahon, K.D., Smith, M.C., 2009. Can the black box be cracked? The augmentation of microbial ecology by high-resolution, automated sensing technologies. ISME Journal 3 (8), 881–888.
Sinsabaugh, R.L., Findlay, S., 1995. Microbial production, enzyme activity, and carbon turnover in surface sediments of the Hudson River estuary. Microbial Ecology 30 (2), 127–141.
Steele, J.H., Henderson, E.W., 1992. A simple model for plankton patchiness. Journal of Plankton Research 14 (10), 1397–1403.
Stemberger, R.S., Gilbert, J.J., 1985. Body size, food concentration, and population growth in planktonic rotifers. Ecology 66 (4), 1151–1159.
Sterner, R.W., Hessen, D.O., 1994. Algal nutrient limitation and the nutrition of aquatic herbivores. Annual Review of Ecology and Systematics 25, 1–29.
Stewart, K.M., 1976. Oxygen deficits, clarity, and eutrophication in some Madison lakes. Internationale Revue gesamten Hydrobiologie 61 (5), 16.
Torrence, C., Compo, G.P., 1998. A practical guide to wavelet analysis. Bulletin of the American Meteorological Society 79 (1), 61–78.
Trolle, D., Hamilton, D.P., Pilditch, C.A., Duggan, I.C., Jeppesen, E., 2011. Predicting the effects of climate change on trophic status of three morphologically varying lakes: implications for lake restoration and management. Environmental Modelling & Software 26 (4), 354–370.
Trolle, D., Skovgaard, H., Jeppesen, E., 2008. The Water Framework Directive: setting the phosphorus loading target for a deep lake in Denmark using the 1D lake ecosystem model DYRESM-CAEDYM. Ecological Modelling 219 (1–2), 138–152.
Ukeles, R., 1961. The effect of temperature on the growth and survival of several marine algal species. Biological Bulletin 120 (2), 255–264.
Urabe, J., Watanabe, Y., 1990. Influence of food density on respiration rate of 2 crustacean plankters, Daphnia galeata and Bosmina longirostris. Oecologia 82 (3), 362–368.
Ventura, M., Camarero, L., Buchcaca, T., Bartumeus, F., Livingstone, D.M., Catalan, J., 2000. The main features of seasonal variability in the external forcing and dynamics of a deep mountain lake (Redo, Pyrenees). Journal of Limnology 59 (1), 97–108.
Vos, R.J., Hakvoort, J.H.M., Jordans, R.W.J., Ibelings, B.W., 2003. Multiplatform optical monitoring of eutrophication in temporally and spatially variable lakes. Science of the Total Environment 312 (1–3), 221–243.
Wanninkhof, R., 1992. Relationship between wind-speed and gas-exchange over the ocean. Journal of Geophysical Research-Oceans 97 (C5), 7373–7382.
Wetzel, R.G., 2001. Limnology: Lake and River Ecosystems, third ed. Academic Press, San Diego.
Wiebe, P.H., Boyd, S., Cox, J.L., 1975. Relationships between zooplankton displacement volume, wet weight, dry weight, and carbon. Fishery Bulletin 73 (4), 777–786.
Yuan, H.L., 2007. Development of a Non-hydrostatic Model and Its Application to Two Akes in Madison, WI, Civil and Environmental Engineering. University of Wisconsin-Madison, Madison, p. 232.
Zohary, unpublished data (after Gal, et al., 2009).